Supplementary Information For:

An aluminium-organic framework unveiling ultra-sensitive fluorometric detection of pesticide paraoxon-methyl and pharmaceutical drug azathioprine in fruits, vegetables, and wastewater

*Arindam Sarma, Subhrajyoti Ghosh and Shyam Biswas**

Department of Chemistry, Indian Institute of Technology Guwahati, 781039 Assam, India

E-mail address: sbiswas@iitg.ac.in

Materials and Characterization Methods:

The synthesis and characterisation procedures for 2-((2-hydroxy-4-methoxy benzyl) amino) terephthalic acid linker was followed by previously reported procedure.[1] All the chemicals were purchased from commercial sources and used without further purification. Attenuated Total Reflectance Infrared (ATR-IR) spectroscopy data were recorded in the region 400-4000 cm^{-1} at room temperature with the Perkin Elmer Spectrum ATR-IR spectrometer. The following indications were used to indicate the corresponding absorption bands: very strong (vs), strong (s), medium (m), weak (w), shoulder (sh) and broad (br). Thermogravimetric (TG) experiments were carried out with a heating rate of 4 °C min^{-1} under N_2 atmosphere using a SDT Q600 thermogravimetric analyser. Powder X-ray diffraction (PXRD) data were collected in transmission mode using Rigaku Smartlab X-ray diffractometer with Cu-*K*α radiation (λ = 1.54056 Å), 40 kV of operating voltage and 125 mA of operating current. Specific surface area for N_2 sorption was calculated on a Quantachrome Autosorb iQMP gas sorption analyser at -196 °C. FE-SEM images were collected with a Zeiss (Sigma 300) scanning electron microscope. FE-TEM images were collected with JEOL transmission electron microscope having model number 2100F. Fluorescence emission studies were performed at room temperature using a HORIBA JOBIN YVON Fluoromax-4 spectrofluorometer. Pawley refinement was carried out using Materials Studio software.[2] Computational analysis was performed by using the B3LYP function and the Pople diffuse basis set 6-31G+(d,p) in Gaussian 09W software.[3] The DICVOL program incorporated within STOE's WinXPow software package was used to determine the lattice parameters.[4]

Preparation of MOF (1′) Suspension for Fluorescence Titration Experiment:

The probe **1′** (4 mg) was collected in a 5 mL glass vial and 4 mL Milli-Q water was added to it to make a homogeneous suspension. Then, the suspension was sonicated for 30 min and kept it for overnight to make the suspension stable. During the fluorescence titration experiment, we used 200 µL of the above-mentioned suspension of **1′,** and 3000 µL of Milli-Q water was added to it in a quartz cuvette. All the fluorescence spectra were collected by exciting the suspension at 328 nm, within the range of 340-600 nm. Paraoxon-methyl and azathioprine solutions were prepared by dissolving in methanol and DMSO, respectively. The aforementioned solutions were added to the suspension of MOF and the photoluminescence emission responses were recorded in the same range.

Fluorometric Detection of Azathioprine in Human Blood Serum Sample:

From the right arm vein of a healthy human, 10 mL of blood sample was collected. The sample was centrifuged at 10,000 rpm for 15 min to obtain blood plasma, from which the light-yellow blood serum was collected and stored in a Falcon tube at -20 °C. To conduct fluorescence detection experiments, varying concentrations of azathioprine were added to different aliquots of the human blood serum sample containing MOF suspension.

Fluorometric Detection of Azathioprine in Human Urine Sample:

A 10 mL urine sample was collected from a healthy individual and treated with 500 mL of HNO_3 to eliminate any interfering living organisms. The sample was then centrifuged at 8000 rpm for 10 min, and the supernatant was used for the experiments. To conduct fluorescence

experiments, various amounts of azathioprine were added to the urine samples containing MOF suspension.

Calculation of Corrected Fluorescence Emission Intensity:

The corrected fluorescence intensity was calculated using the following equation:

$$\frac{F_{corrected}}{F_{observed}} = \frac{2.3dA_{exc}}{1-10^{-dA_{exc}}} 10^{gA_{em}} \frac{2.3sA_{em}}{1-10^{-sA_{em}}}$$

where $F_{observed}$ is the maximum fluorescence intensity; Fcorrected is the corrected fluorescence intensity, which is the fluorescence intensity obtained after removing the inner filter effect; A_{exc} and A_{em} represent the absorbance at the excitation wavelength of probe (λ_{exc} = 328 nm) and maximum emission wavelength (λ_{em} = 428 nm), respectively.; d is the width of the quartz cell (d =1.0 cm); g is the distance between the edges of the cuvette and the excitation beam (0.4 cm in this case); s is the thickness of excitation light (s = 0.1 cm).

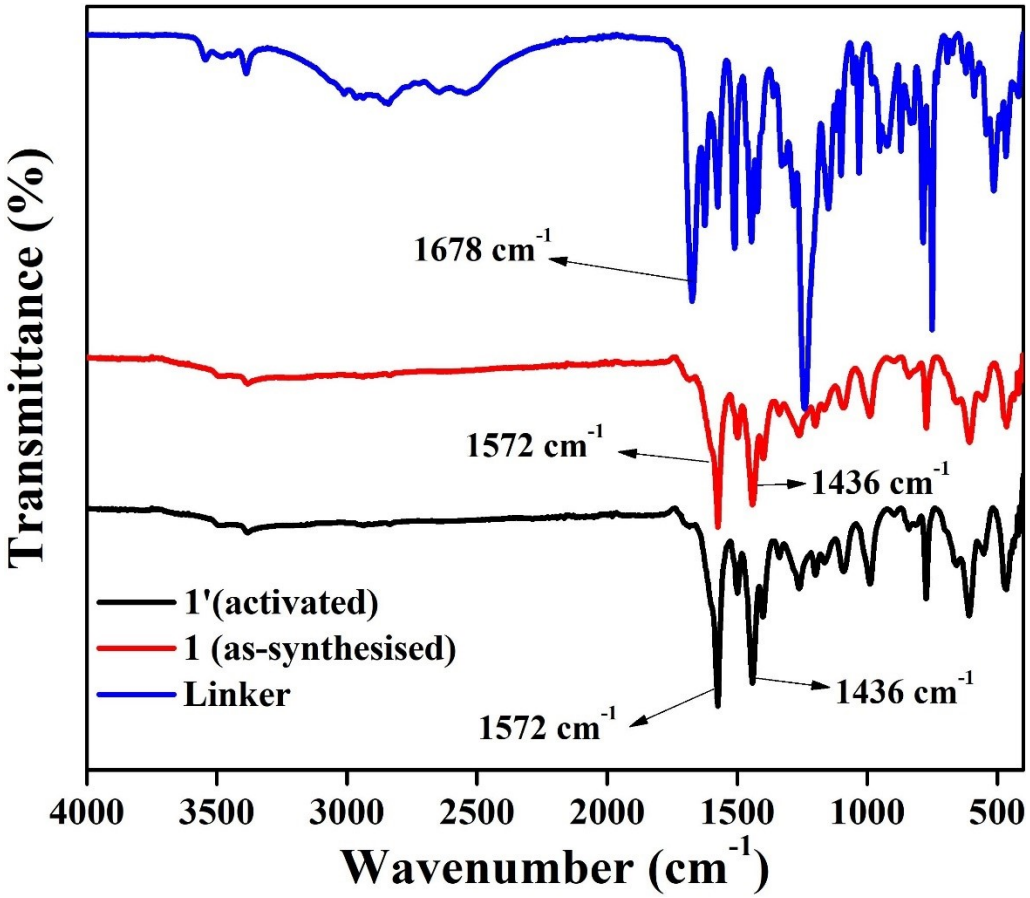

Figure S1. ATR-IR spectra of (a) 2-((2-hydroxy-4-methoxy benzyl amino) terephthalic acid linker (b) as-synthesised **1** (red) and (b) activated **1′** (black).

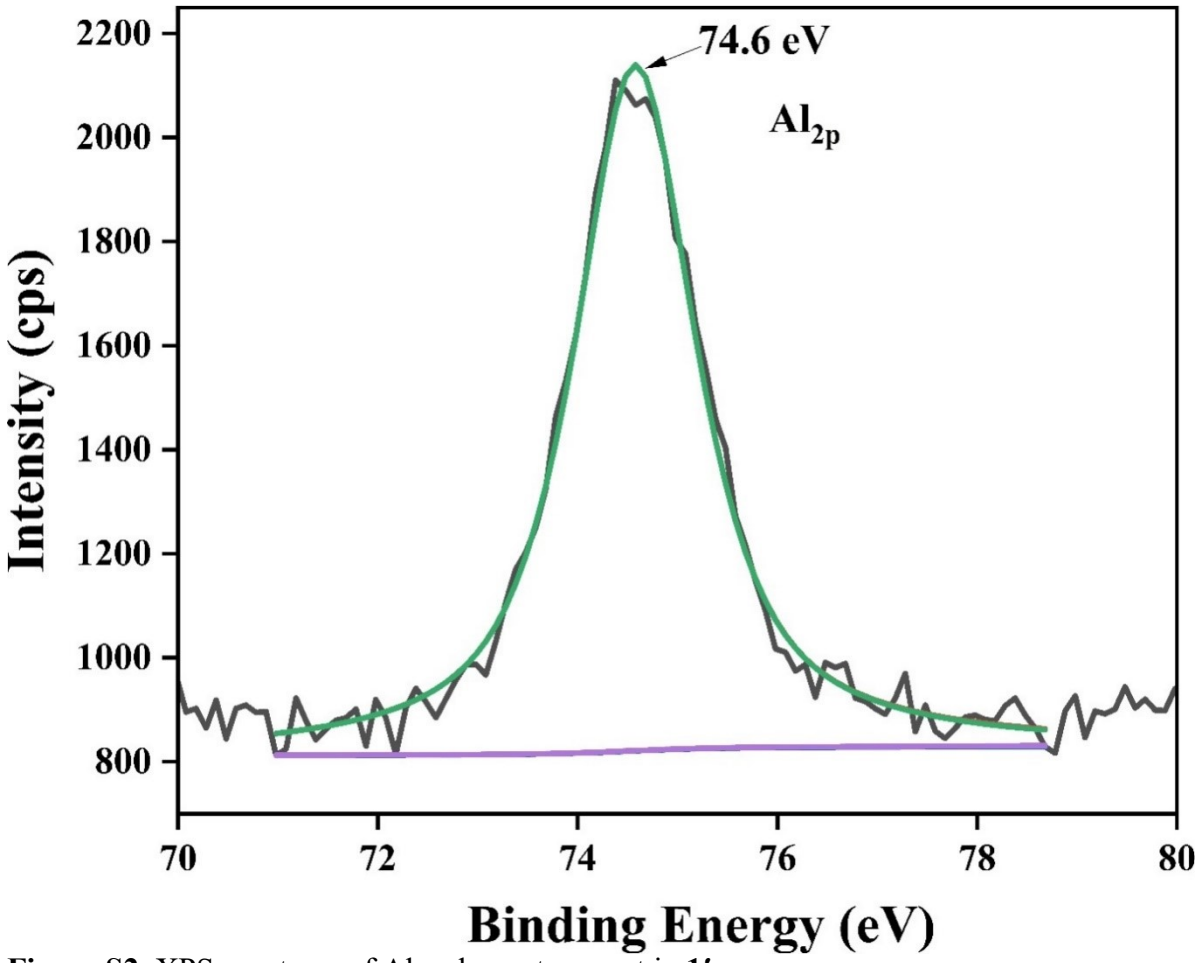

Figure S2. XPS spectrum of Al_{2p} element present in **1′**.

Table S1. Unit cell parameters of **1** compared with those of reported Al-MIL-53.

Compound Name	**[Al(OH)(L)]·0.5H$_2$O (1)** (this work)	Al-MIL-53 (reported)[5]
Crystal System	Orthorhombic	Orthorhombic
a ≠ b ≠ c (Å)	16.590(14) ≠ 12.942(8) ≠ 6.588(5)	16.893(3) ≠ 12.592(2) ≠ 6.623(2)
α = β = γ (°)	90	90
V (Å^3)	1414.6(22)	1408.8 (5)
Radiation	Cu Kα1	Cu Kα1

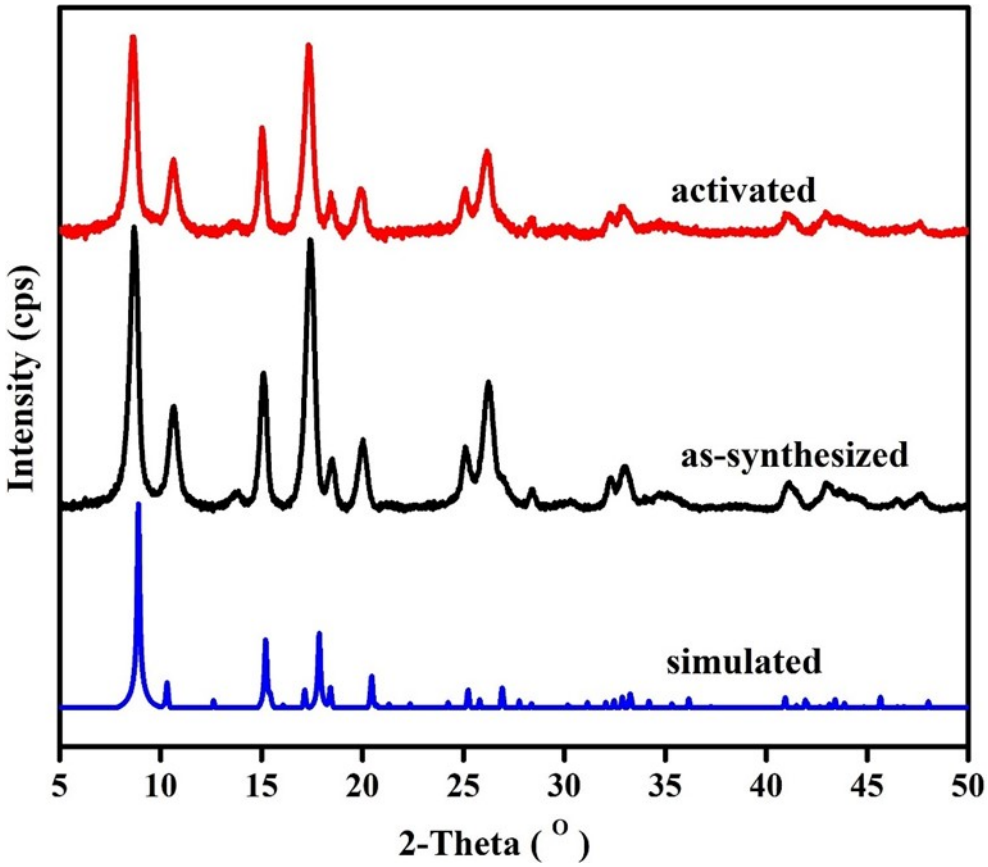

Figure S3. PXRD patterns of simulated (blue), as-synthesized **1** (black) and activated **1′** (red).

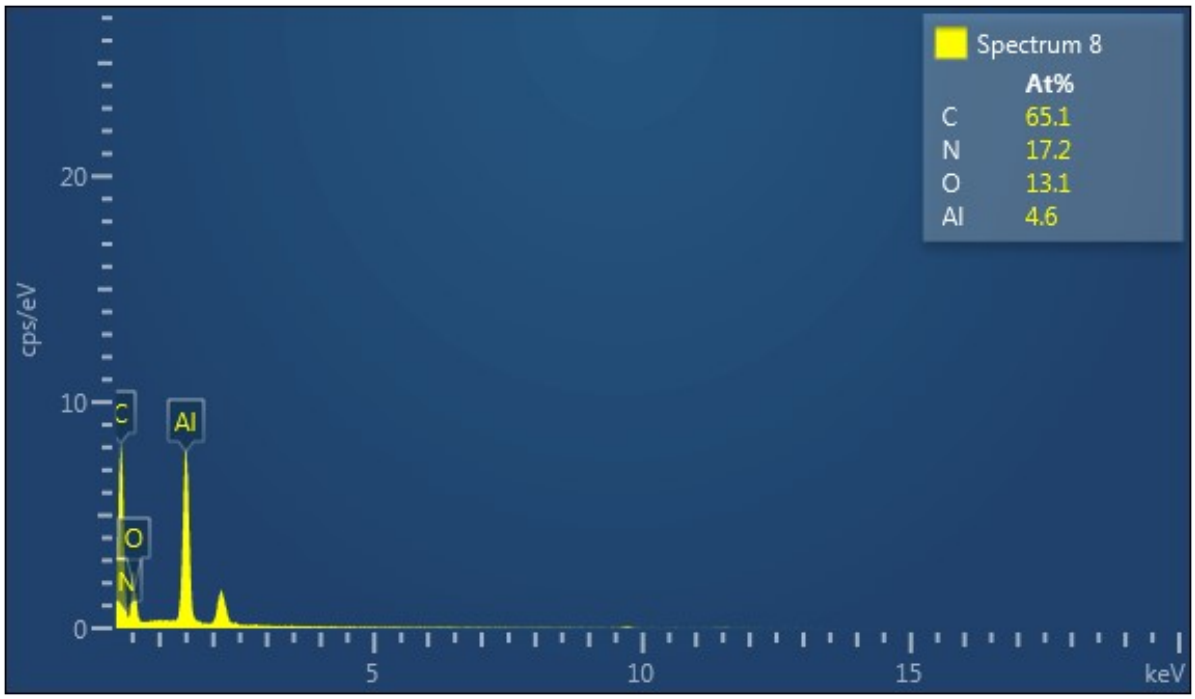

Figure S4. EDX image of **1**.

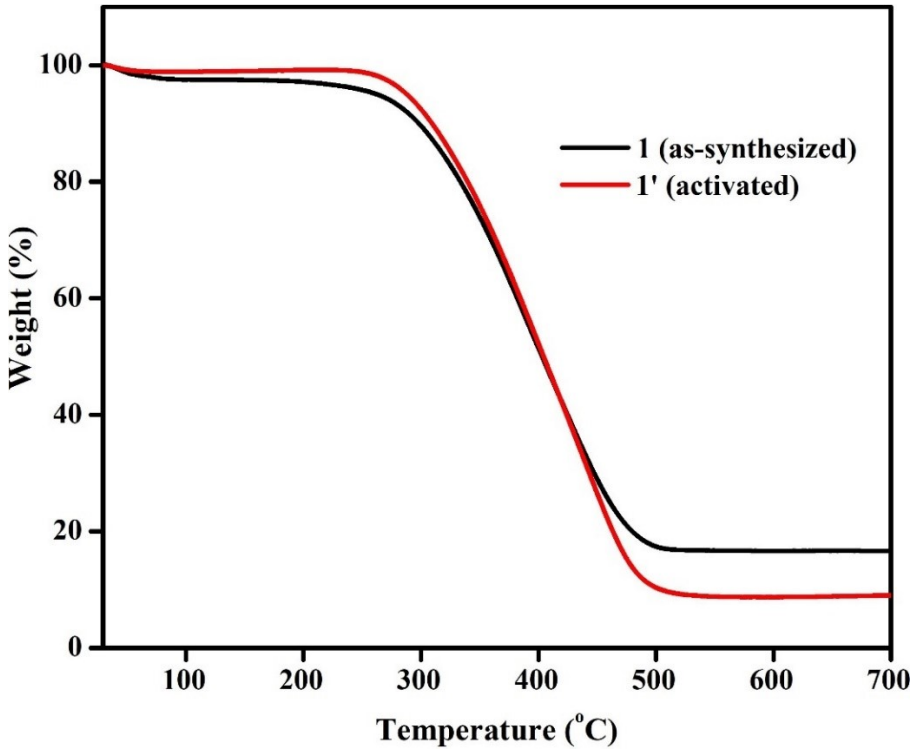

Figure S5. Thermogravimetric analysis curves of as-synthesized **1** (black) and activated **1′** (red) recorded under N_2 atmosphere in the temperature range of 30-700 °C with a heating rate of 4 °C min^{-1}.

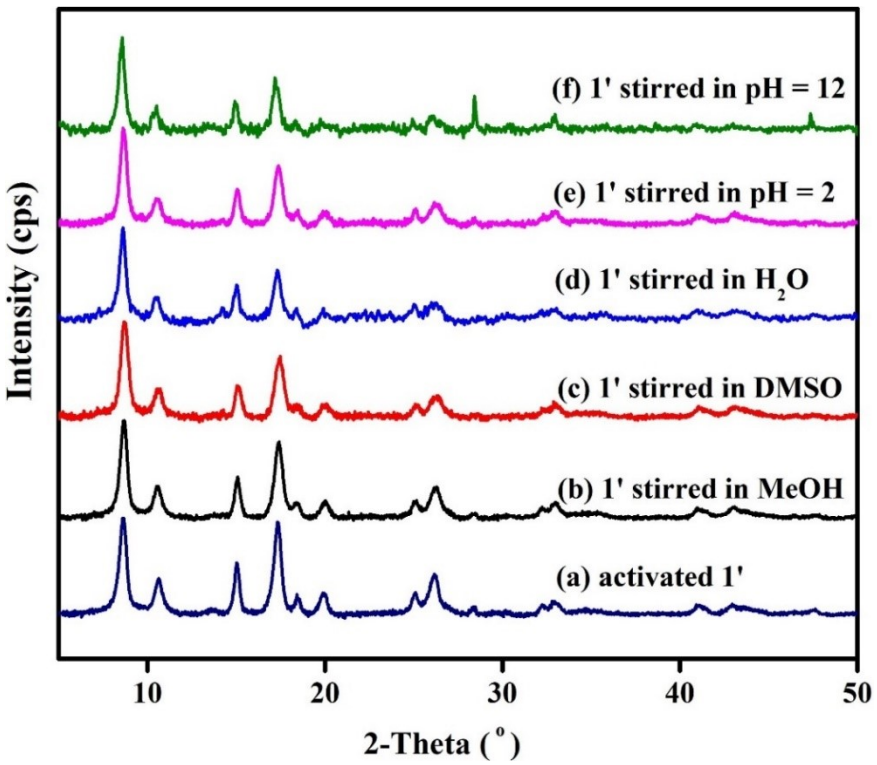

Figure S6. PXRD patterns of (a) non-treated **1'** and **1'** after stirring in (b) MeOH, (c) DMSO, (d) H_2O, (e) pH = 2, and (f) pH = 12 for 24 h.

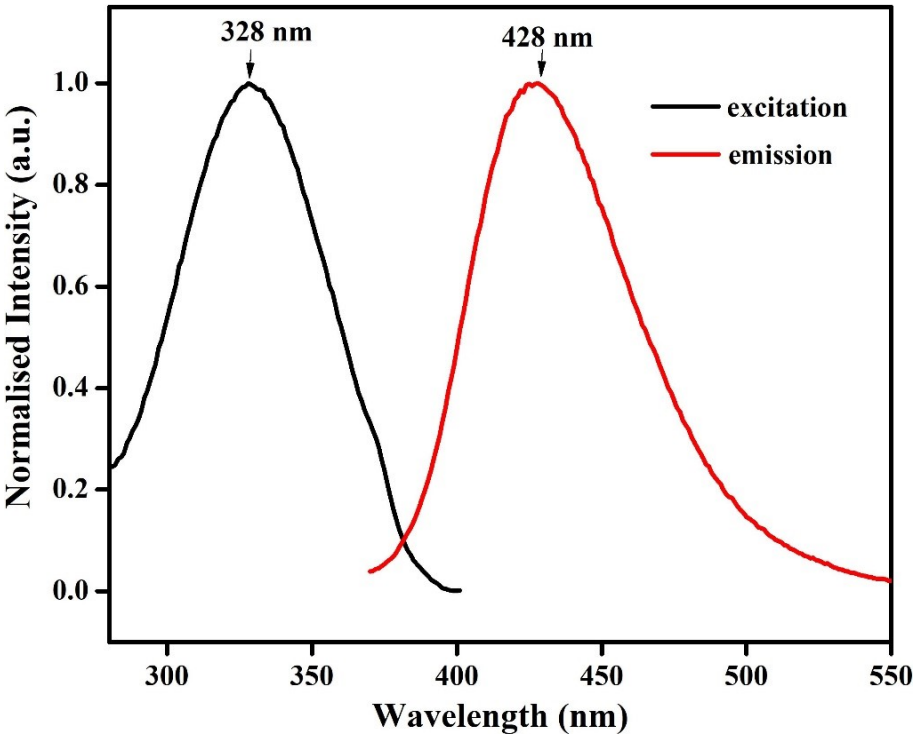

Figure S7. Excitation (black) and emission (red) spectra of **1′** in water.

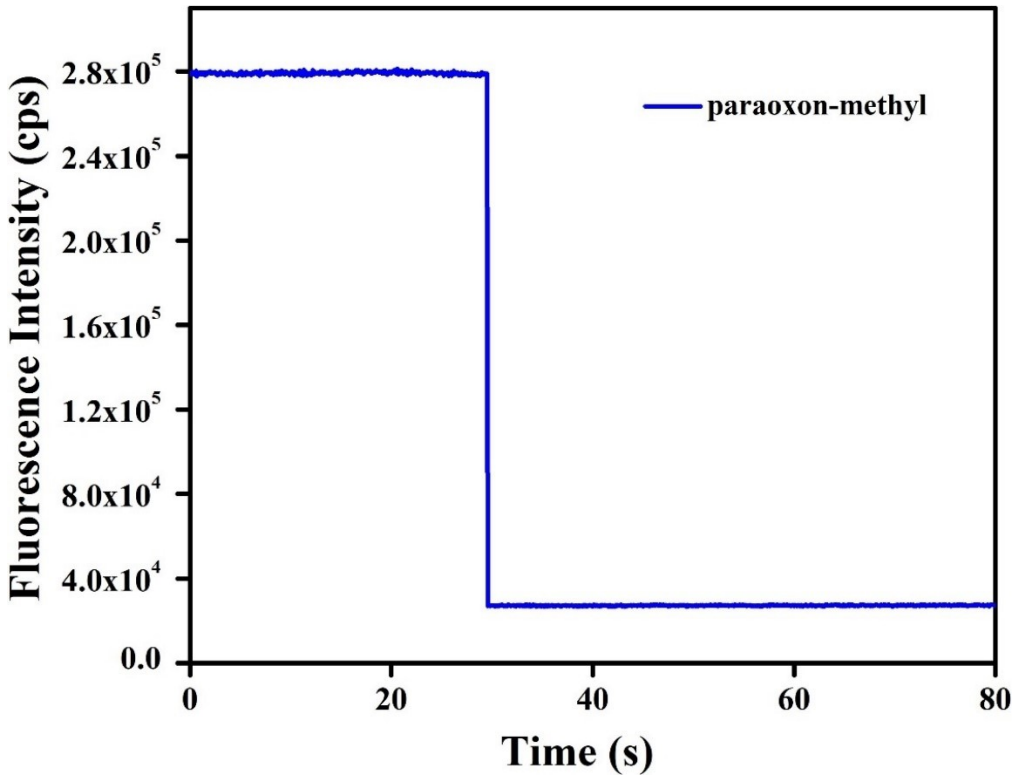

Figure S8. Time-dependent variation in the fluorescence spectrum of **1′** after addition of 300 µL of 10 mM solution of paraoxon-methyl.

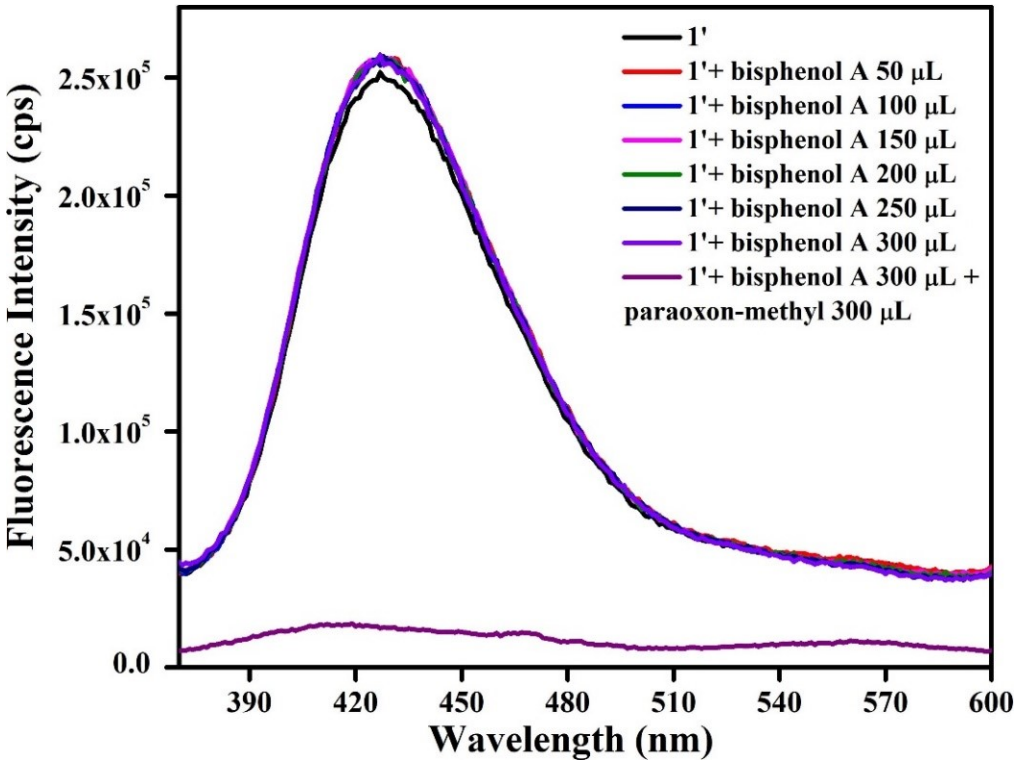

Figure S9. Fluorescence quenching intensity of the aqueous solution of **1′** after gradual addition of 300 µL of 10 mM bisphenol A solution in presence of 300 µL of 10 mM solution of paraoxon-methyl.

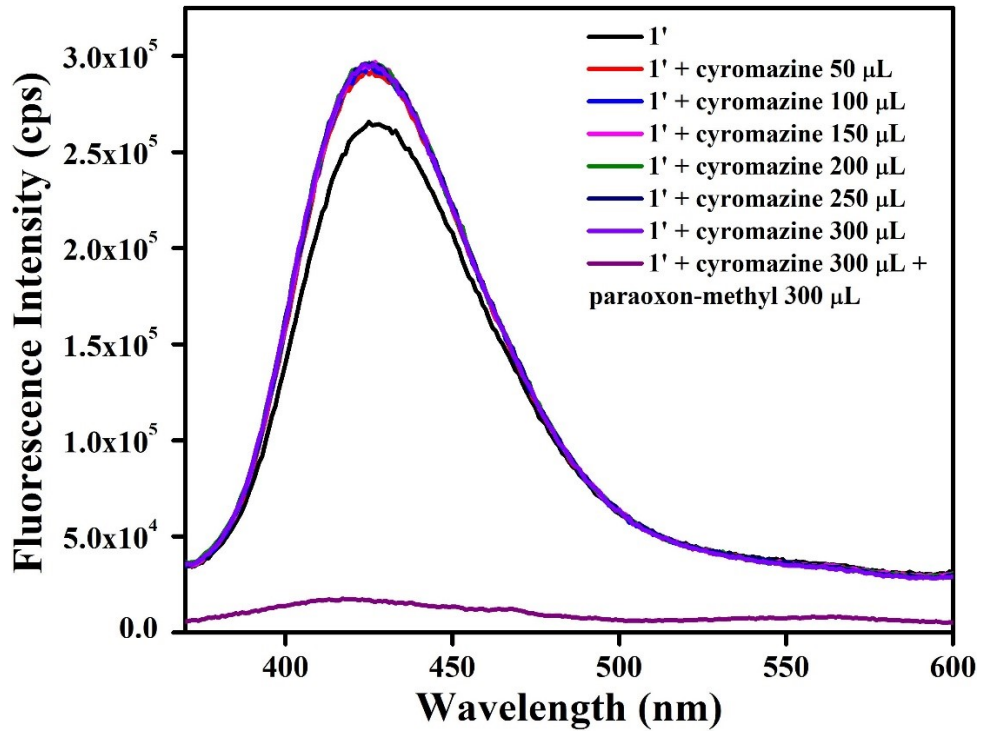

Figure S10. Fluorescence quenching intensity of the aqueous solution of **1′** after gradual addition of 300 µL of 10 mM aqueous cyromazine solution in presence of 300 µL of 10 mM solution of paraoxon-methyl.

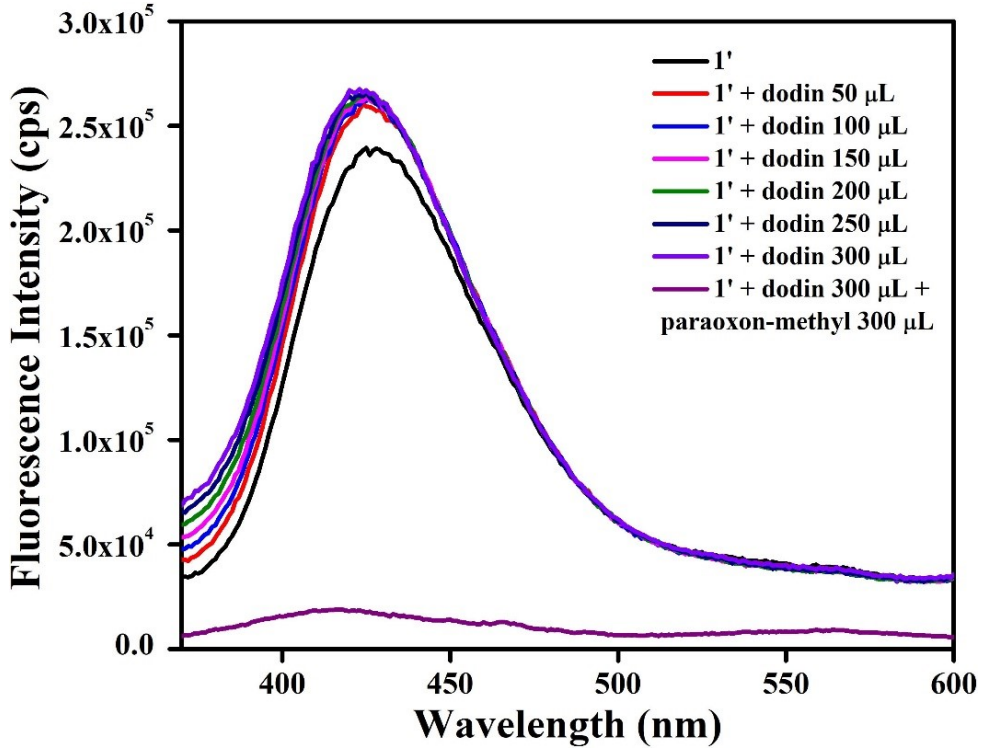

Figure S11. Fluorescence quenching intensity of the aqueous solution of **1′** after gradual addition of 300 µL of 10 mM dodin solution in presence of 300 µL of 10 mM solution of paraoxon-methyl.

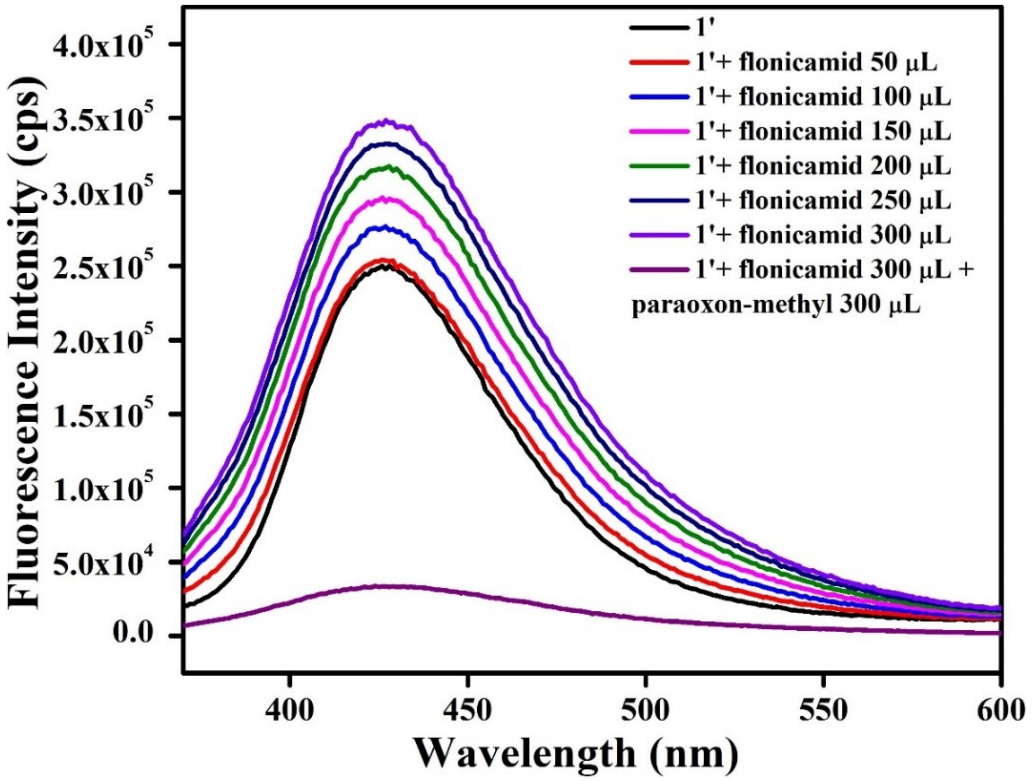

Figure S12. Fluorescence quenching intensity of the aqueous solution of **1′** after gradual addition of 300 µL of 10 mM flonicamid solution in presence of 300 µL of 10 mM solution of paraoxon-methyl.

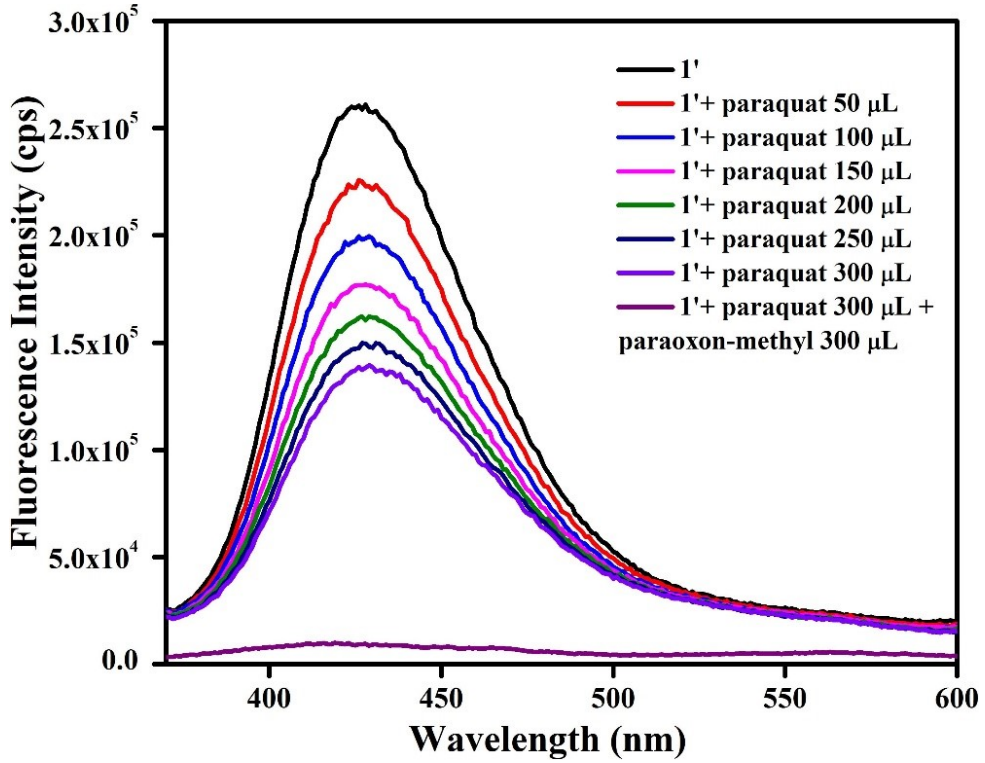

Figure S13. Fluorescence quenching intensity of the aqueous solution of **1′** after gradual addition of 300 µL of 10 mM paraquat solution in presence of 300 µL of 10 mM solution of paraoxon-methyl.

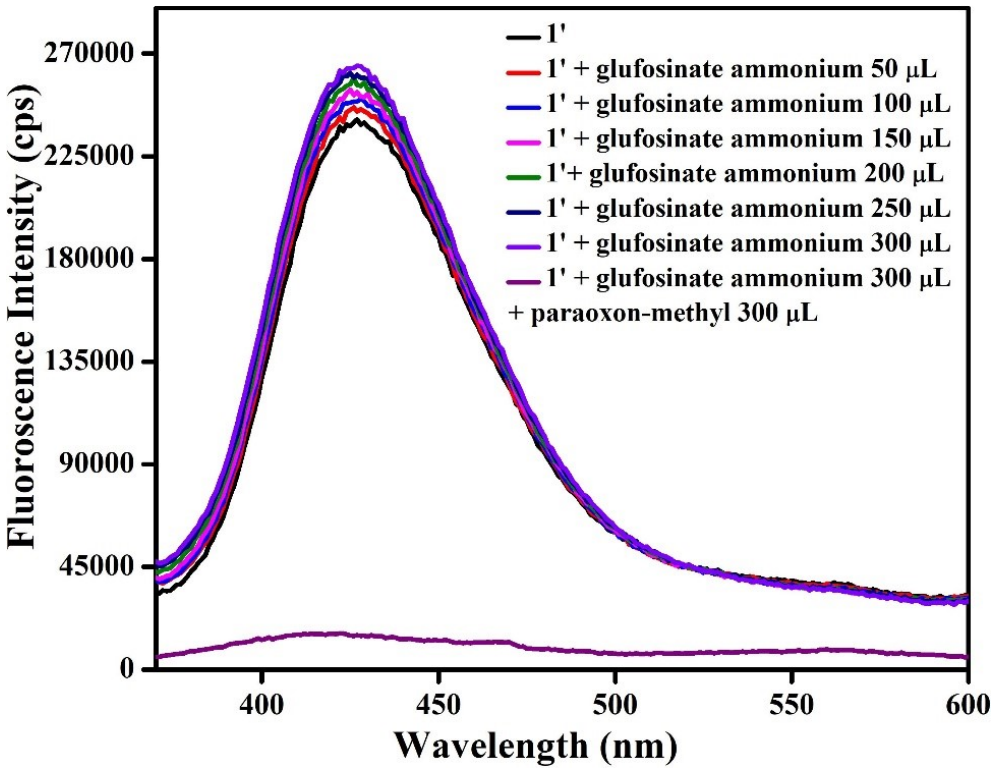

Figure S14. Fluorescence quenching intensity of the aqueous solution of **1′** after gradual addition of 300 µL of 10 mM glufosinate ammonium solution in presence of 300 µL of 10 mM solution of paraoxon-methyl.

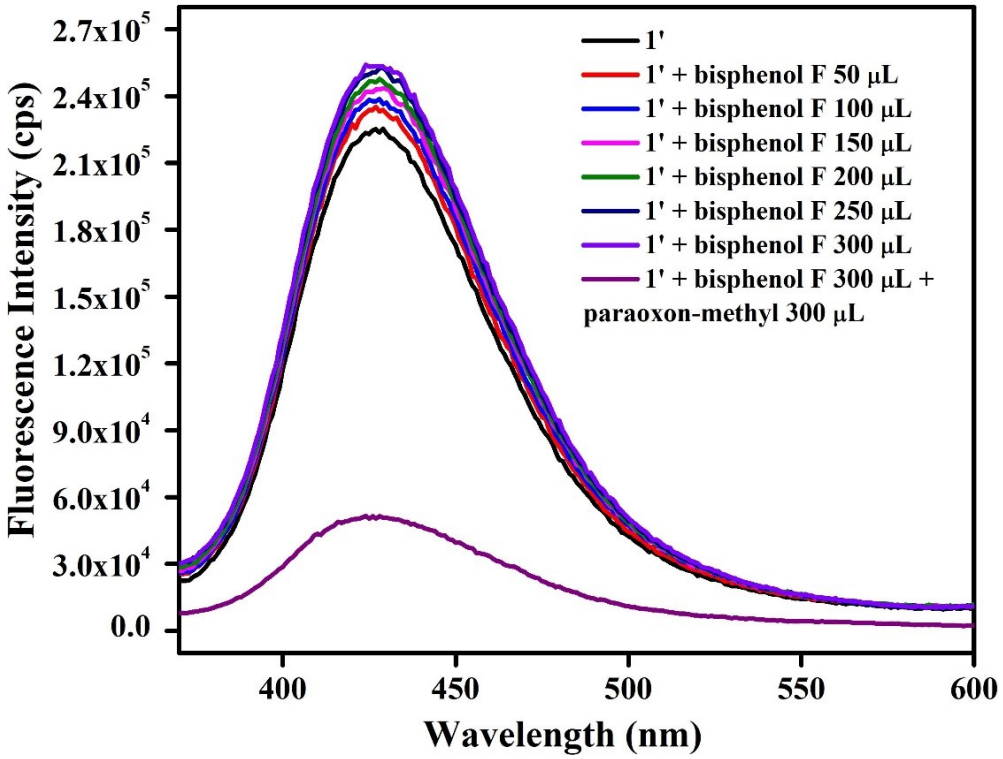

Figure S15. Fluorescence quenching intensity of the aqueous solution of **1′** after gradual addition of 300 µL of 10 mM bisphenol F solution in presence of 300 µL of 10 mM solution of paraoxon-methyl.

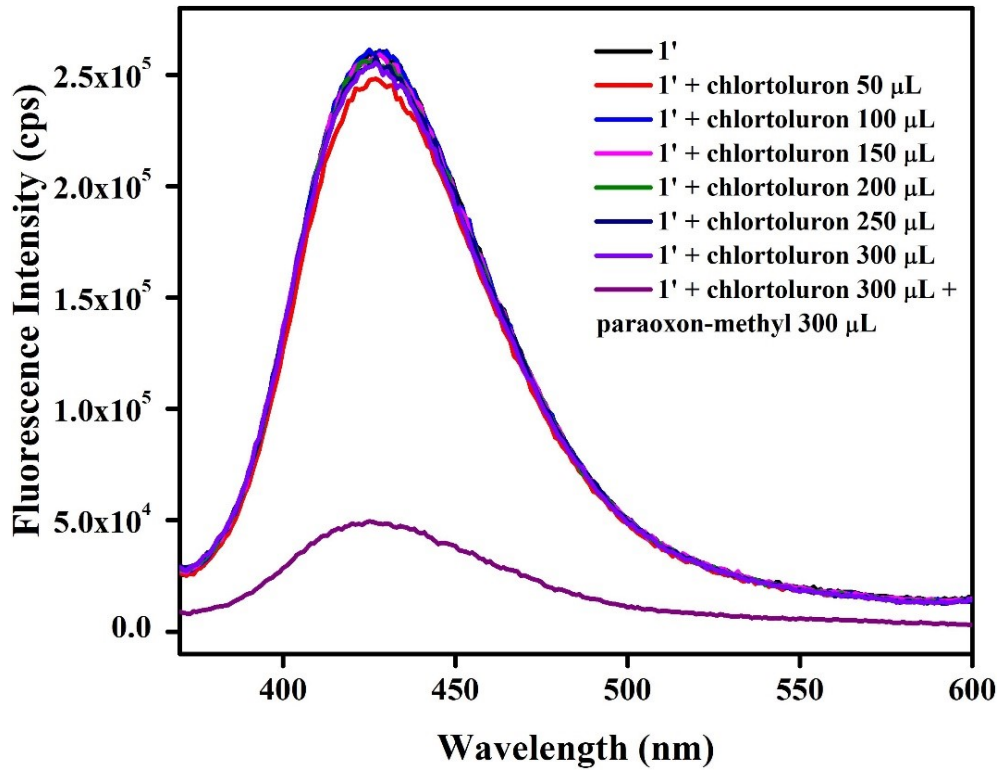

Figure S16. Fluorescence quenching intensity of the aqueous solution of **1′** after gradual addition of 300 µL of 10 mM chlortoluron solution in presence of 300 µL of 10 mM solution of paraoxon-methyl.

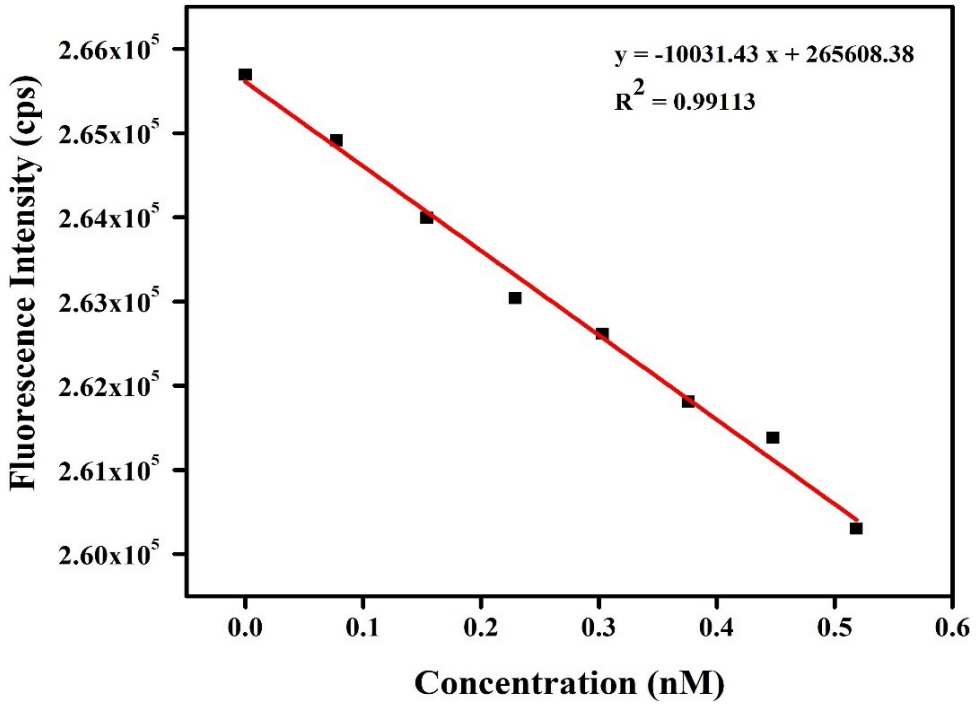

Figure S17. Change of fluorescence intensity of **1'** as a function of the concentration of paraoxon-methyl in water.

Table S2. Comparison of the response time, detection limit, K_{SV} and sensing media used for the reported fluorometric sensors for paraoxon-methyl sensing.

Sl. No.	Probe	Sensing Medium	K_{SV} (M^{-1})	LOD (nM)	Response Time (s)	Ref.
1	B, N CDs	water	-	99.94	120	6
2	C based fluorescent nanocomposite	water	-	1250.00	-	7
3	CdTe / ZnS QDs	water	-	0.65		8
4	Eu-NDC MOF	ethanol	8.05×10^3	85.13	30	9
5	$Ru(bpy)_3^{2+}$ and ThT@ZnCPs	water	-	0.93	3600	10
6	TPE-Peptide	phosphate buffer	-	600.00	900	11
7	**$[Al(OH)(C_{16}H_{13}NO_6)]\cdot 0.5H_2O$**	**water**	**38.5×10^6**	**0.30**	**10**	**this work**

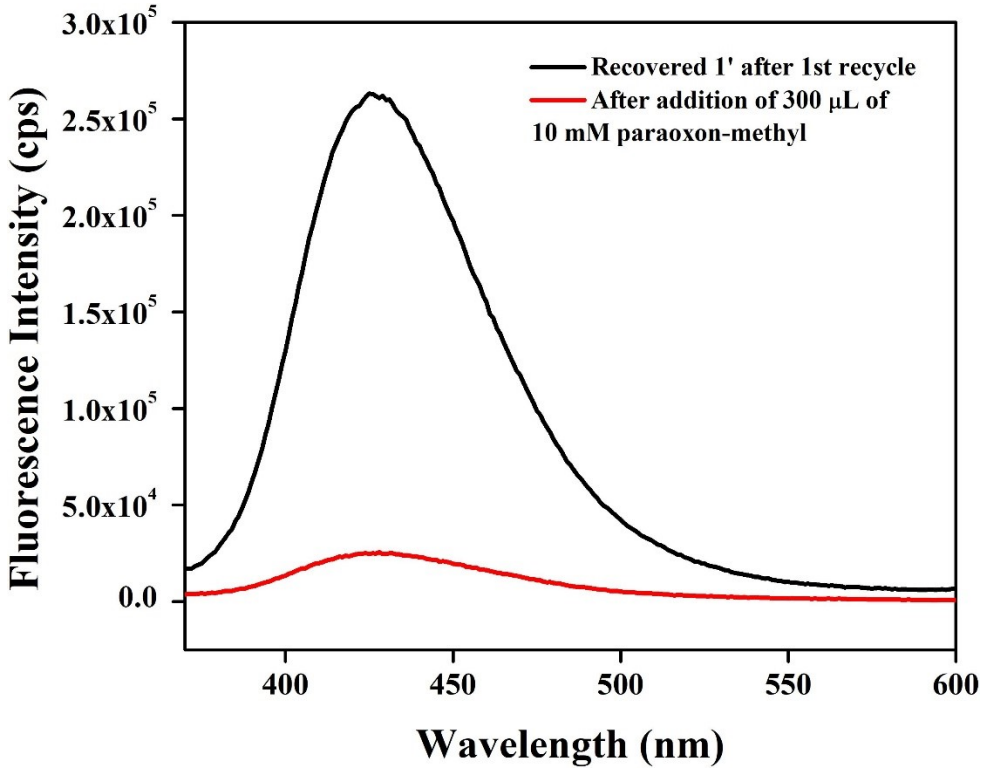

Figure S18. Photoluminescence spectrum for recyclability test of probe **1'** recovered from 1st cycle for the sensing of 10 mM paraoxon-methyl in aqueous medium.

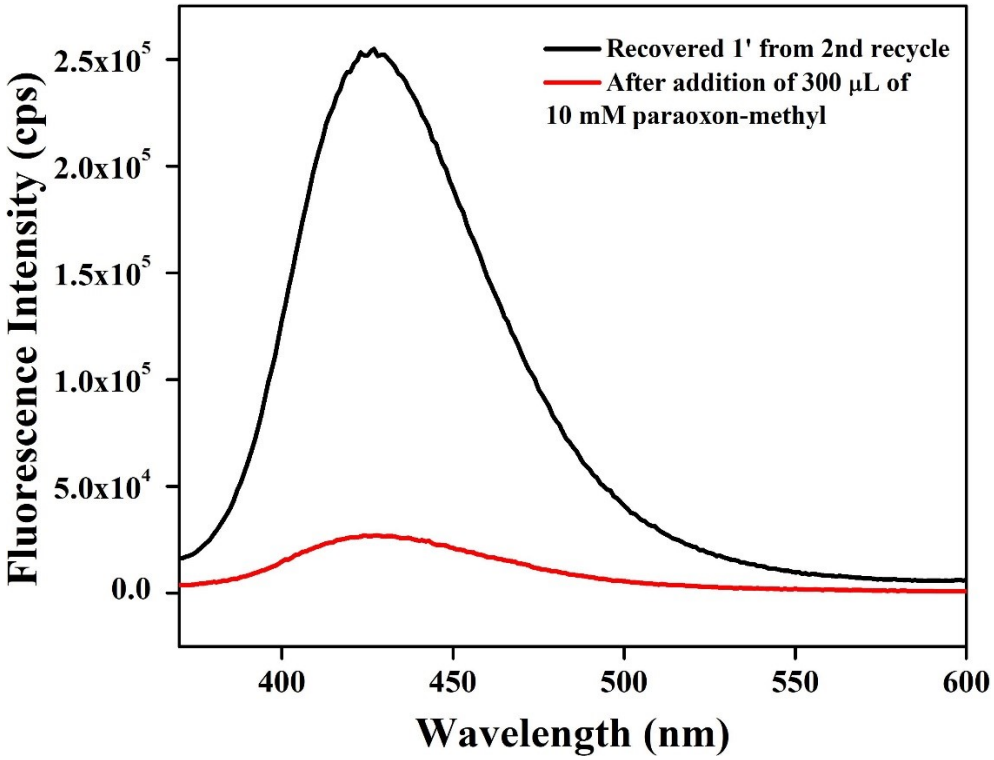

Figure S19. Photoluminescence spectrum for recyclability test of probe **1'** recovered from 2nd cycle for the sensing of 10 mM paraoxon-methyl in aqueous medium.

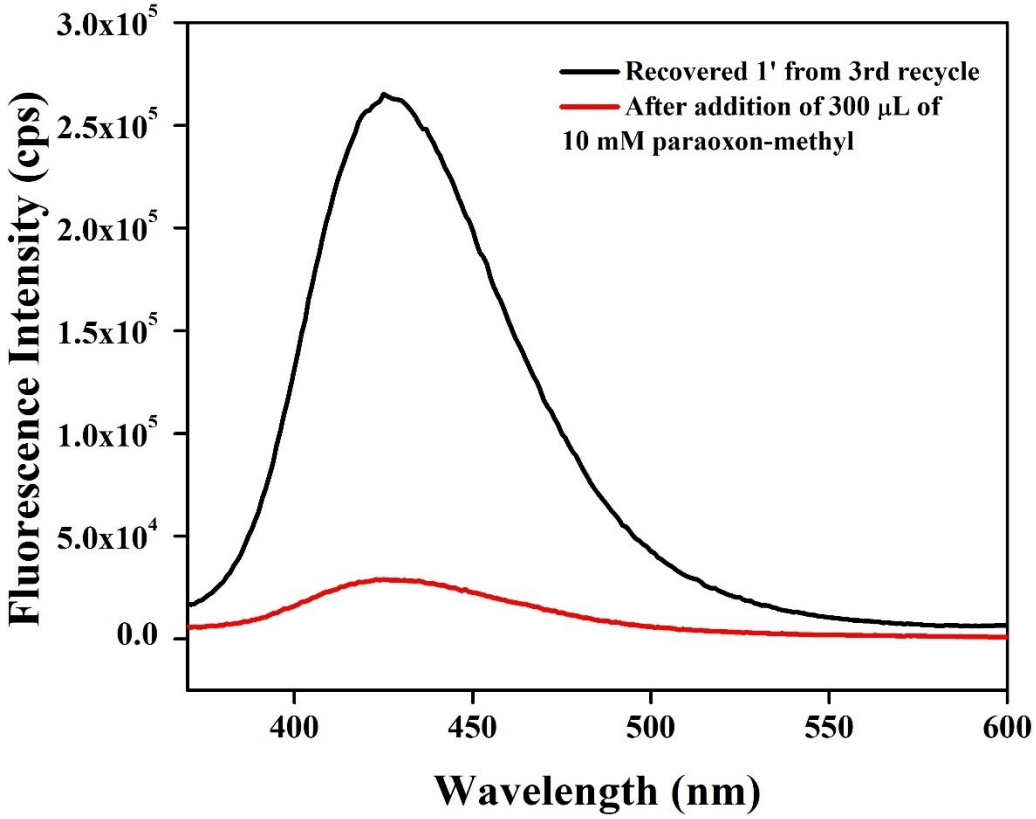

Figure S20. Photoluminescence spectrum for recyclability test of probe **1'** recovered from 3rd cycle for the sensing of 10 mM paraoxon-methyl in aqueous medium.

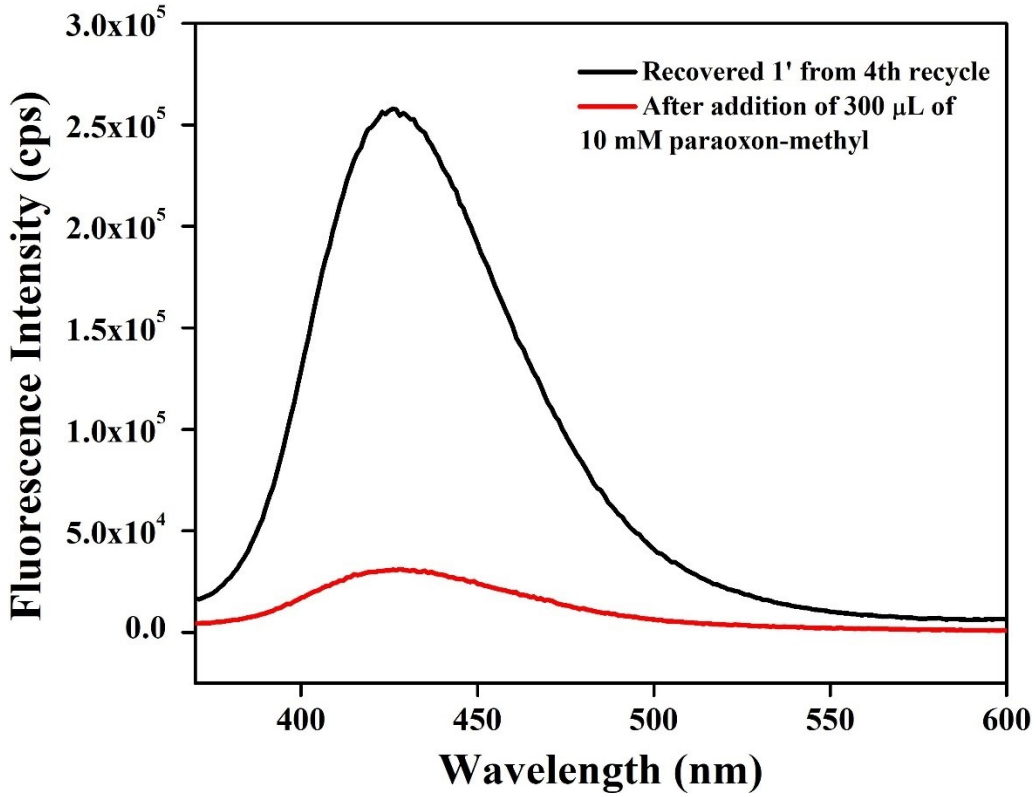

Figure S21. Photoluminescence spectrum for recyclability test of probe **1'** recovered from 4th cycle for the sensing of 10 mM paraoxon-methyl in aqueous medium.

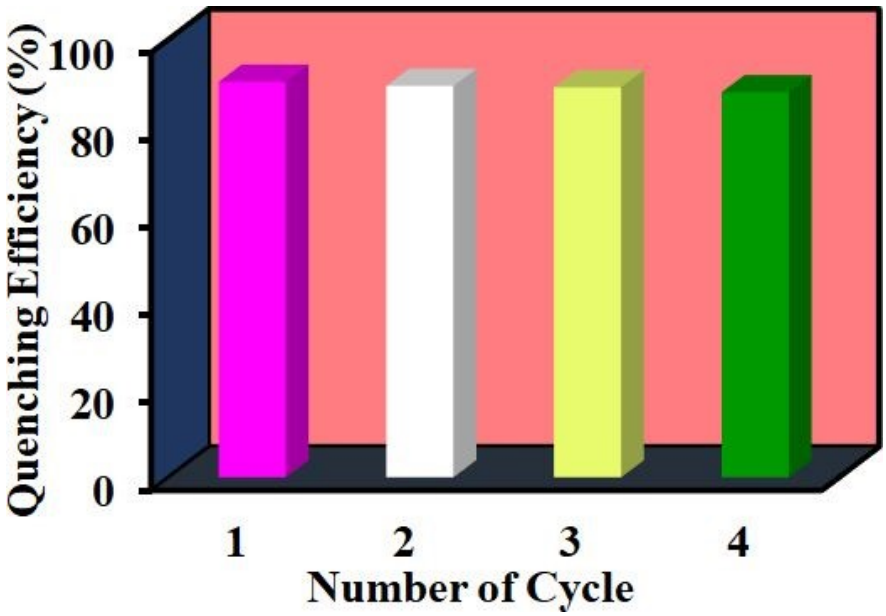

Figure S22. Recyclability test of probe **1'** for the sensing of 10 mM paraoxon-methyl in aqueous medium.

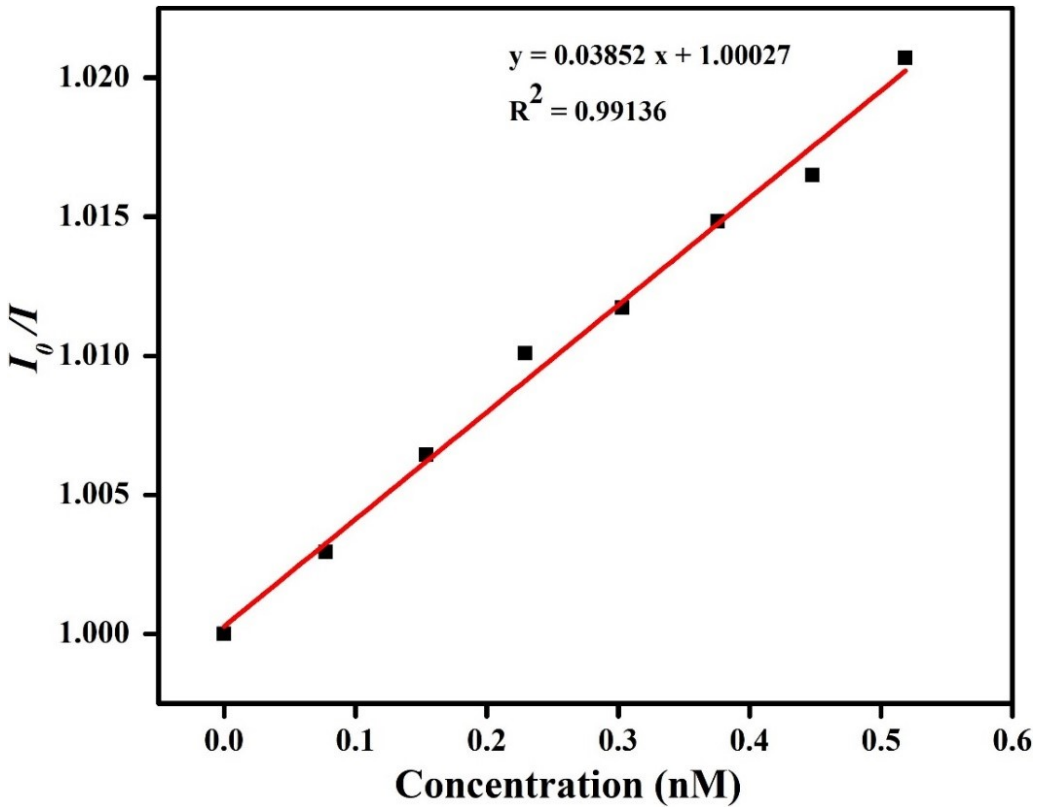

Figure S23. Stern-Volmer plot for the fluorescence quenching of **1'** in presence of paraoxon-methyl in aqueous medium.

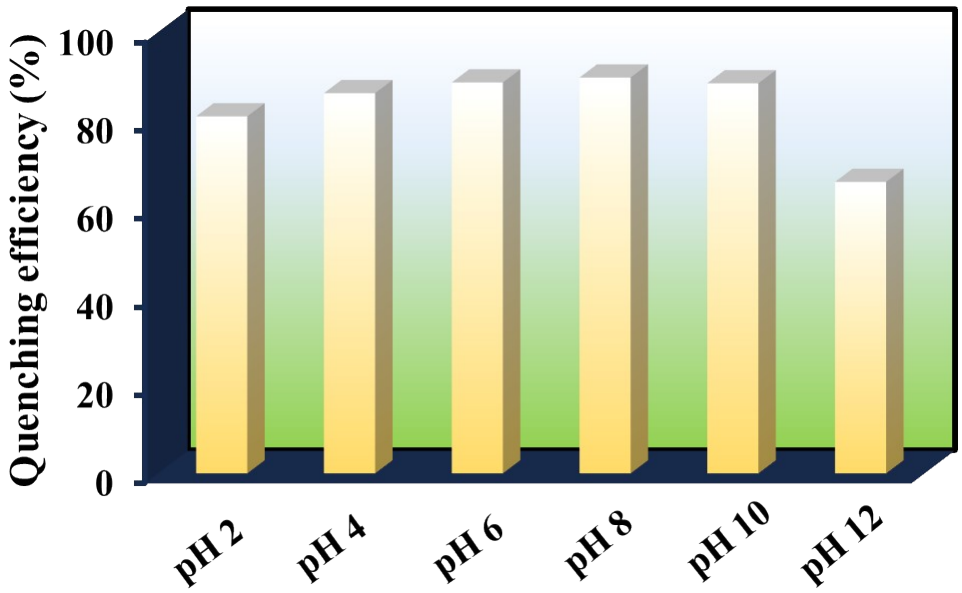

Figure S24. Variation of quenching efficiency after addition of paraoxon-methyl to a suspension of **1'** in aqueous solution of wide range of pH.

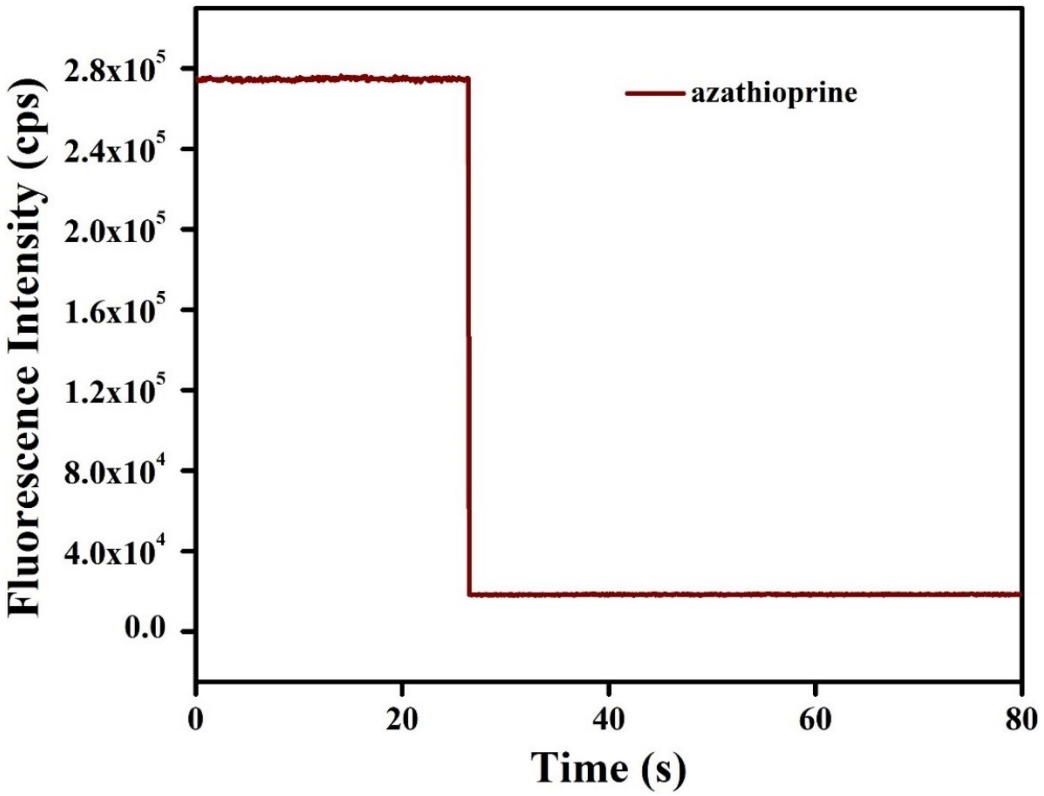

Figure S25. Time-dependent variation in the fluorescence spectrum of **1′** after addition of 300 µL of 5 mM solution of azathioprine.

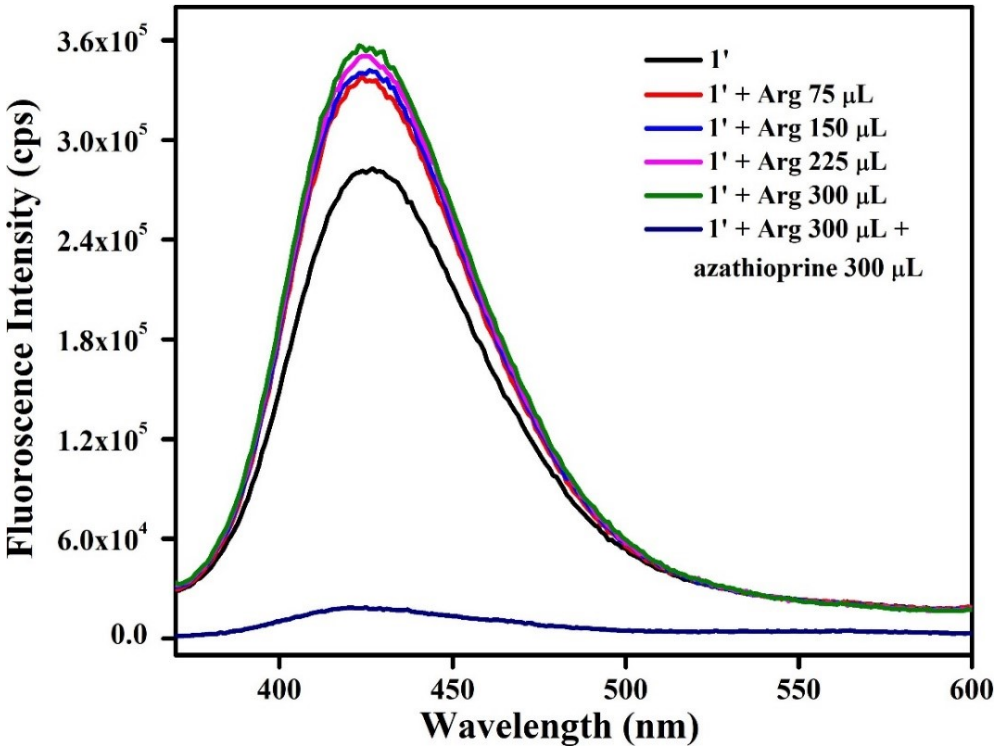

Figure S26. Fluorescence intensity of the aqueous solution of **1′** after gradual addition of 300 µL of 5 mM aqueous arginine solution in the presence of 300 µL of 5 mM solution of azathioprine.

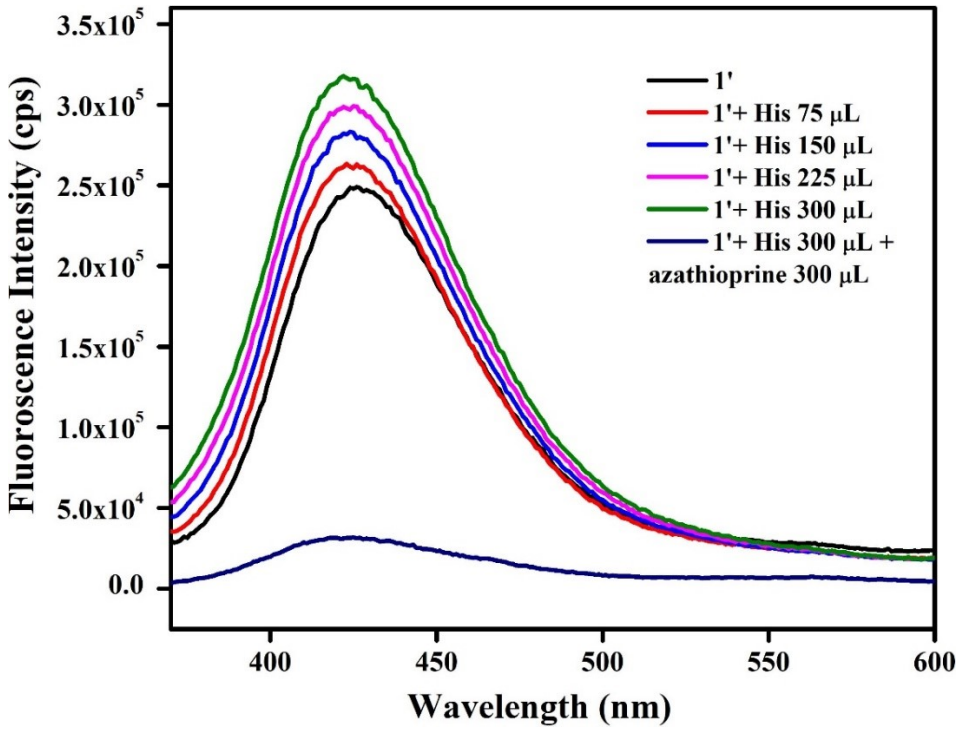

Figure S27. Fluorescence intensity of the aqueous solution of **1′** after gradual addition of 300 µL of 5 mM aqueous histidine solution in presence of 300 µL of 5 mM solution of azathioprine.

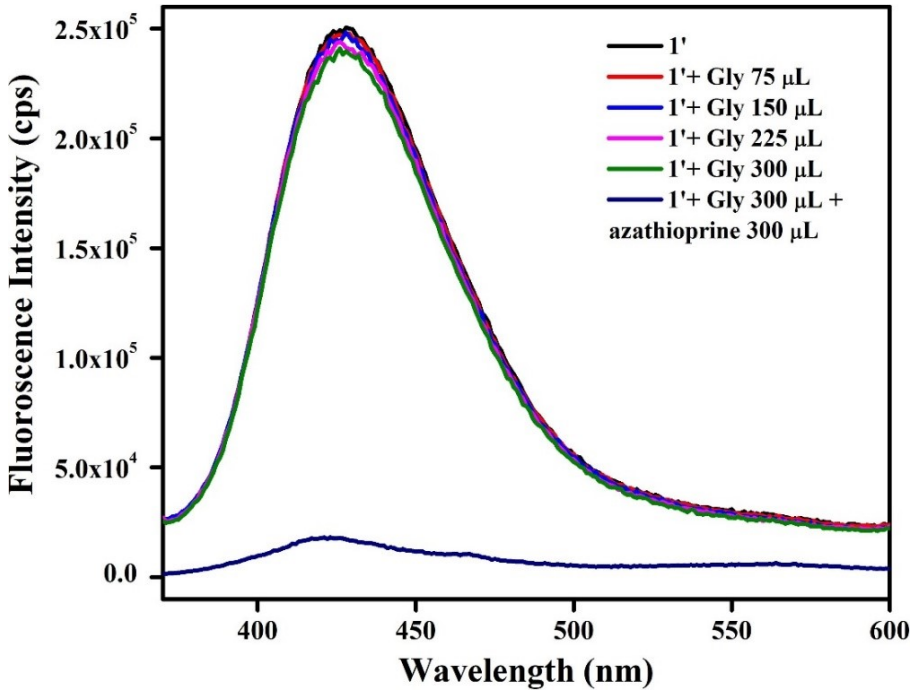

Figure S28. Fluorescence intensity of the aqueous solution of **1′** after gradual addition of 300 µL of 5 mM aqueous glycine solution in presence of 300 µL of 5 mM solution of azathioprine.

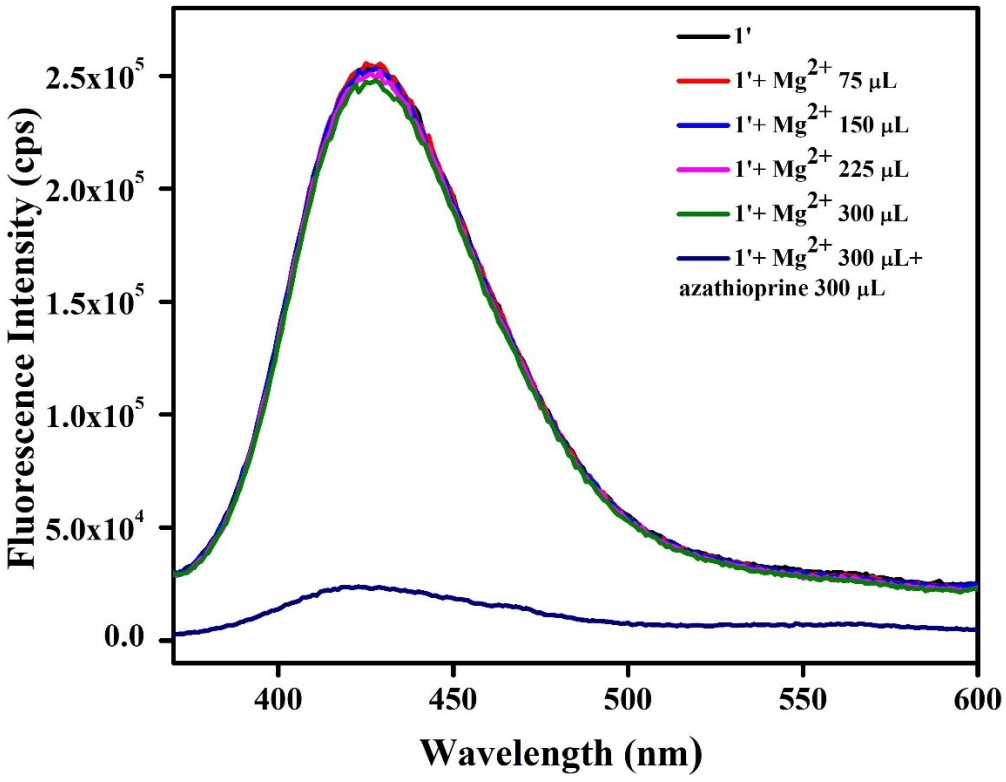

Figure S29. Fluorescence quenching intensity of the aqueous solution of **1′** after gradual addition of 300 µL of 5 mM aqueous Mg^{2+} solution in presence of 300 µL of 5 mM solution of azathioprine.

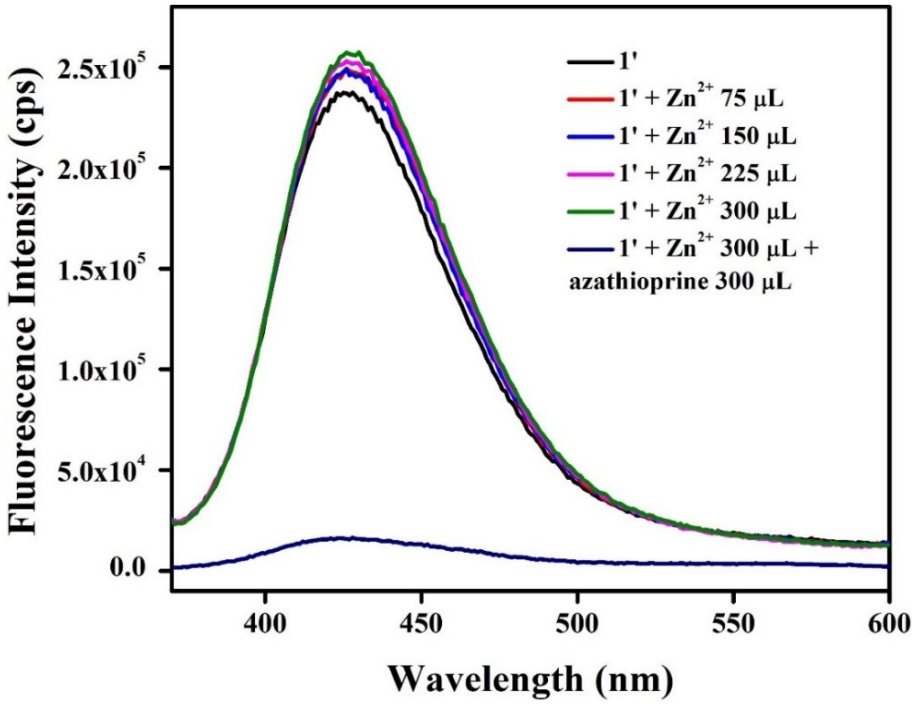

Figure S30. Fluorescence quenching intensity of the aqueous solution of **1′** after gradual addition of 300 µL of 5 mM aqueous Zn^{2+} solution in presence of 300 µL of 5 mM solution of azathioprine.

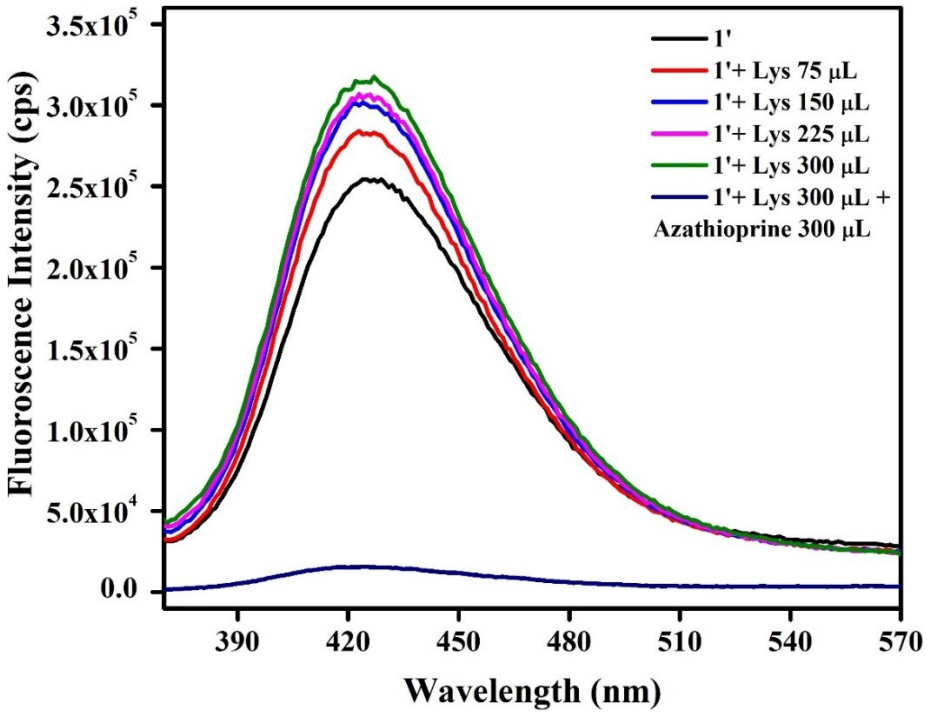

Figure S31. Fluorescence quenching intensity of the solution of **1′** after gradual addition of 300 µL of 5 mM aqueous methionine solution in presence of 300 µL of 5 mM solution of azathioprine.

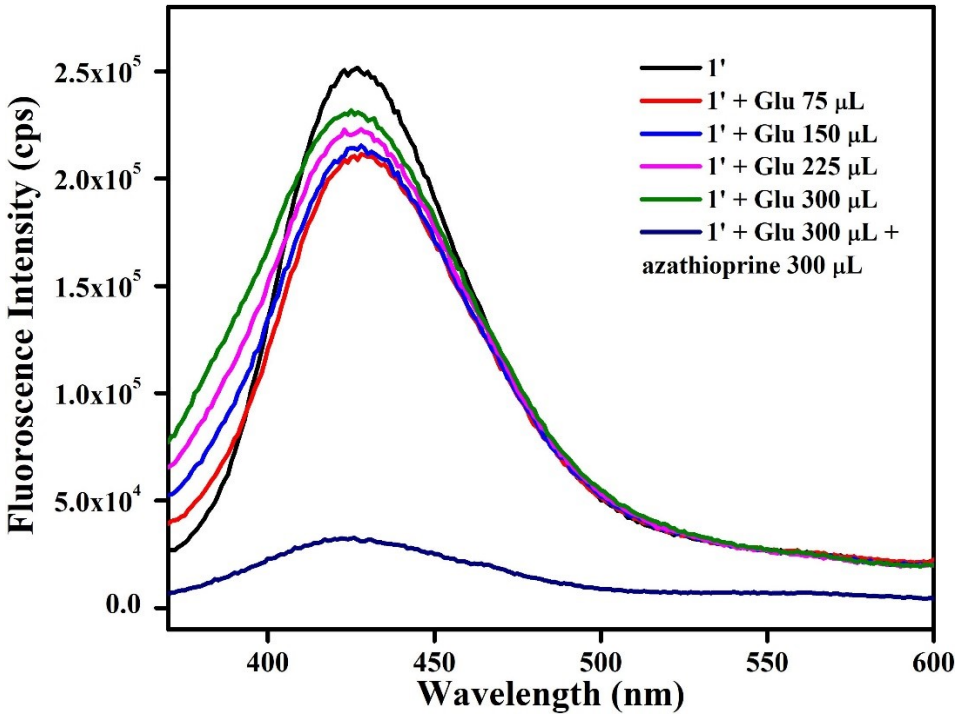

Figure S32. Fluorescence quenching intensity of the aqueous solution of **1′** after gradual addition of 300 µL of 5 mM aqueous glutamic acid solution in presence of 300 µL of 5 mM solution of azathioprine.

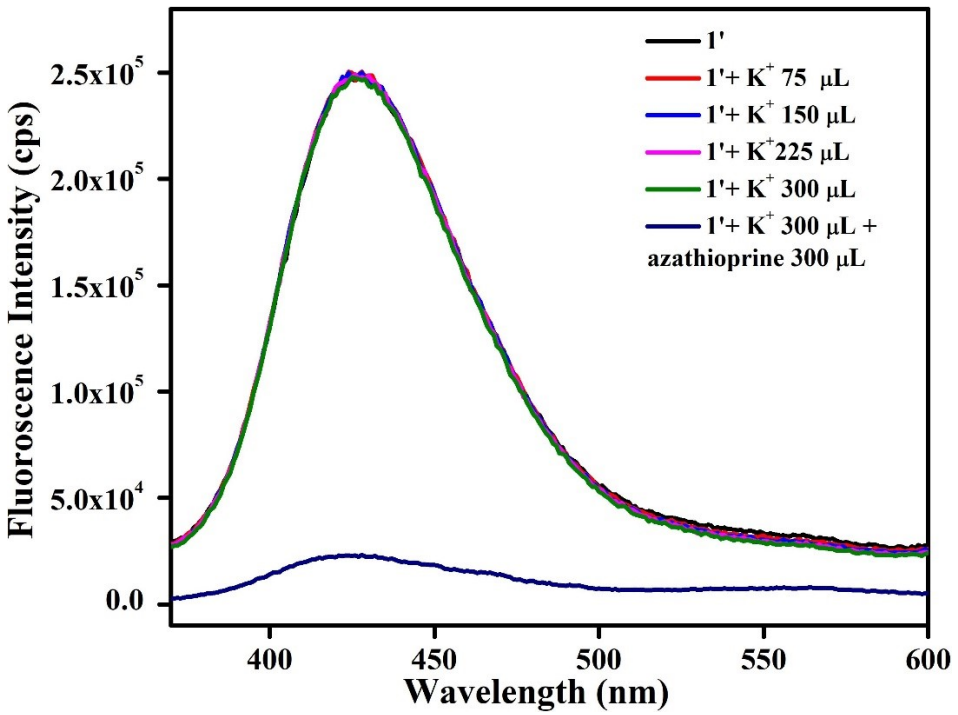

Figure S33. Fluorescence quenching intensity of the aqueous solution of **1′** after gradual addition of 300 µL of 5 mM aqueous K^+ solution in presence of 300 µL of 5 mM solution of azathioprine.

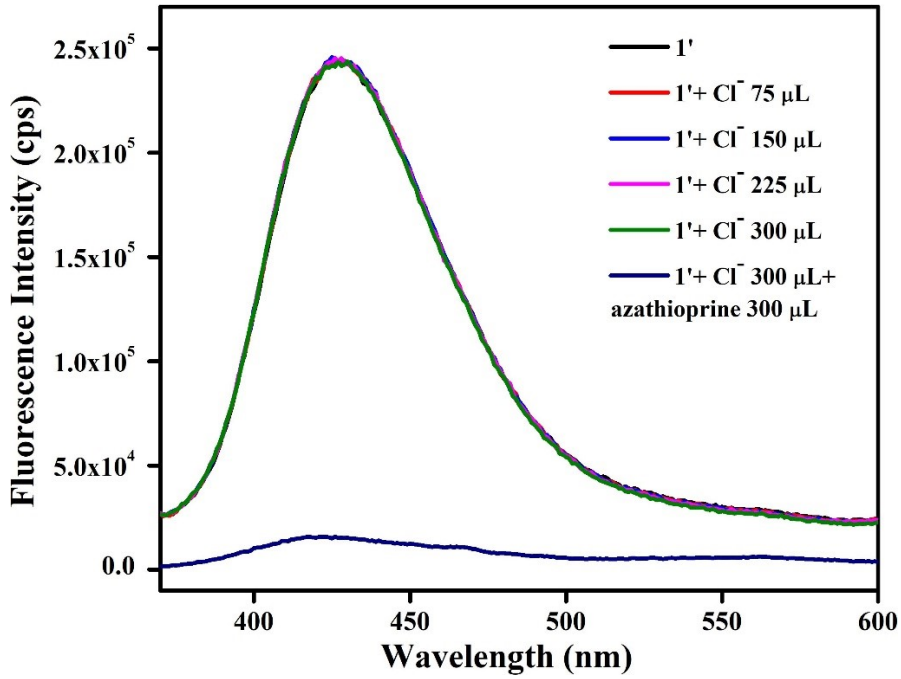

Figure S34. Fluorescence quenching intensity of the aqueous solution of **1′** after gradual addition of 300 µL of 5 mM aqueous Cl^- solution in presence of 300 µL of 5 mM solution of azathioprine.

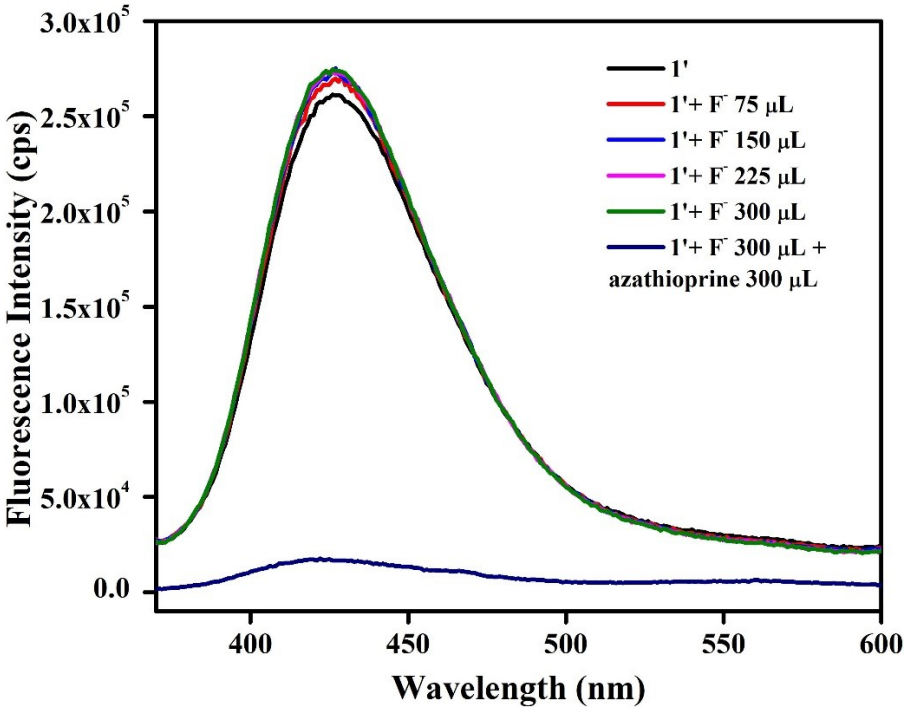

Figure S35. Fluorescence quenching intensity of the aqueous solution of **1′** after gradual addition of 300 µL of 5 mM aqueous F^- solution in presence of 300 µL of 5 mM solution of azathioprine.

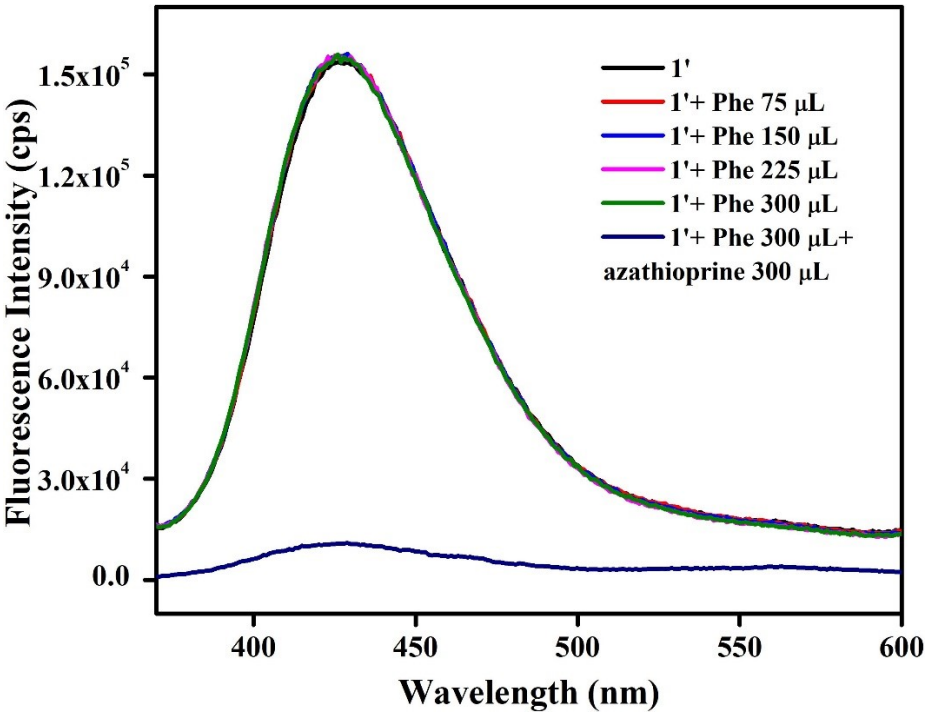

Figure S36. Fluorescence quenching intensity of the aqueous solution of **1′** after gradual addition of 300 µL of 5 mM aqueous phenylalanine solution in presence of 300 µL of 5 mM solution of azathioprine.

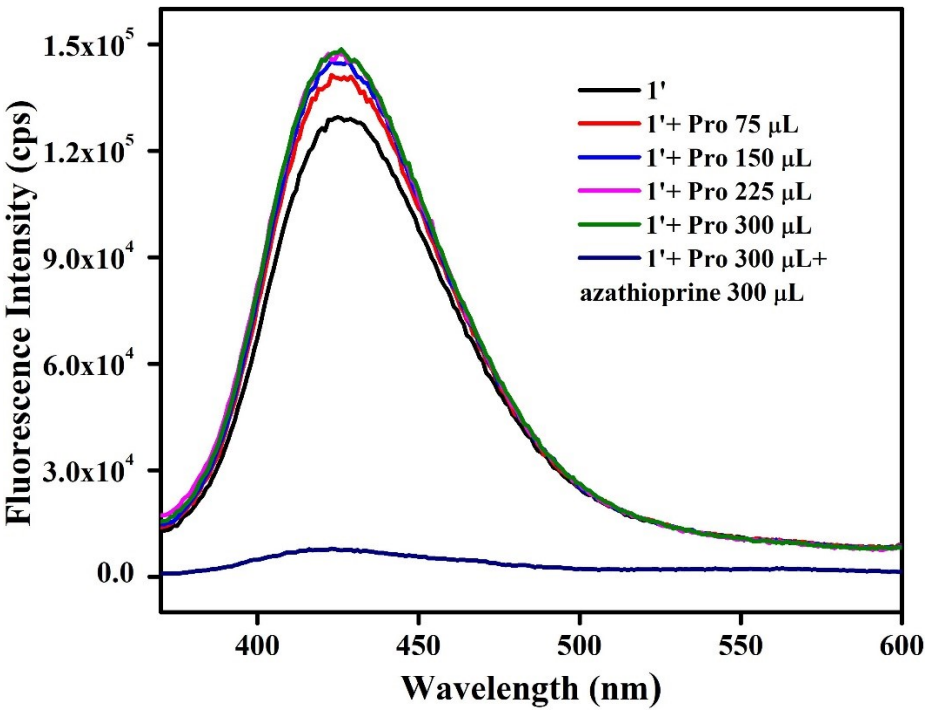

Figure S37. Fluorescence quenching intensity of the aqueous solution of **1′** after gradual addition of 300 µL of 5 mM aqueous proline solution in presence of 300 µL of 5 mM solution of azathioprine.

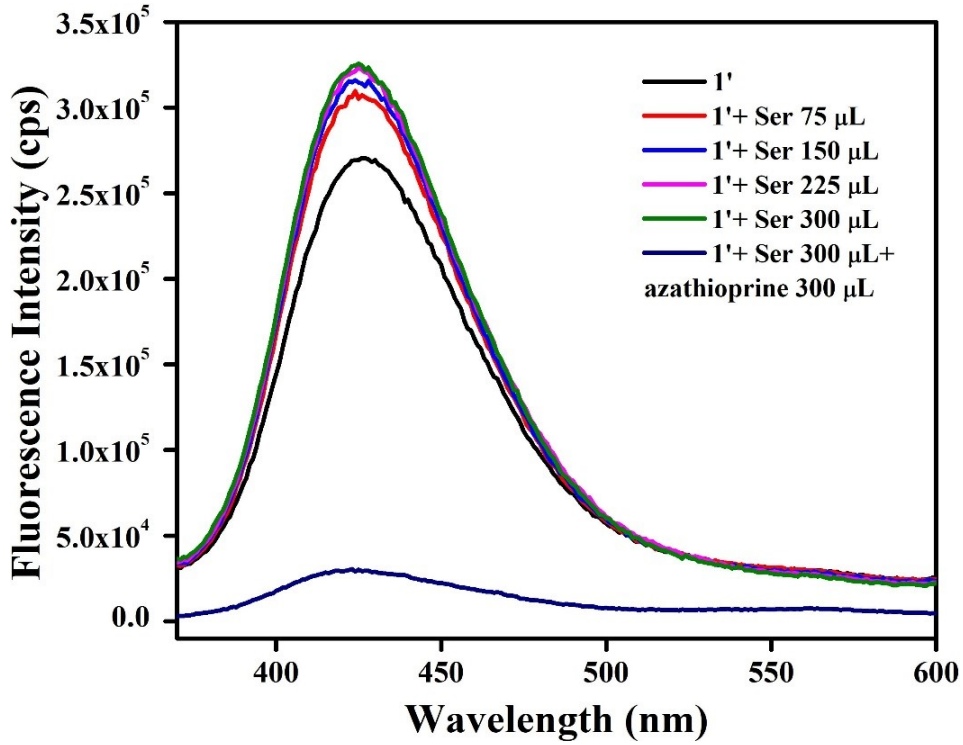

Figure S38. Fluorescence quenching intensity of the aqueous solution of **1′** after gradual addition of 300 µL of 5 mM aqueous serine solution in presence of 300 µL of 5 mM solution of azathioprine.

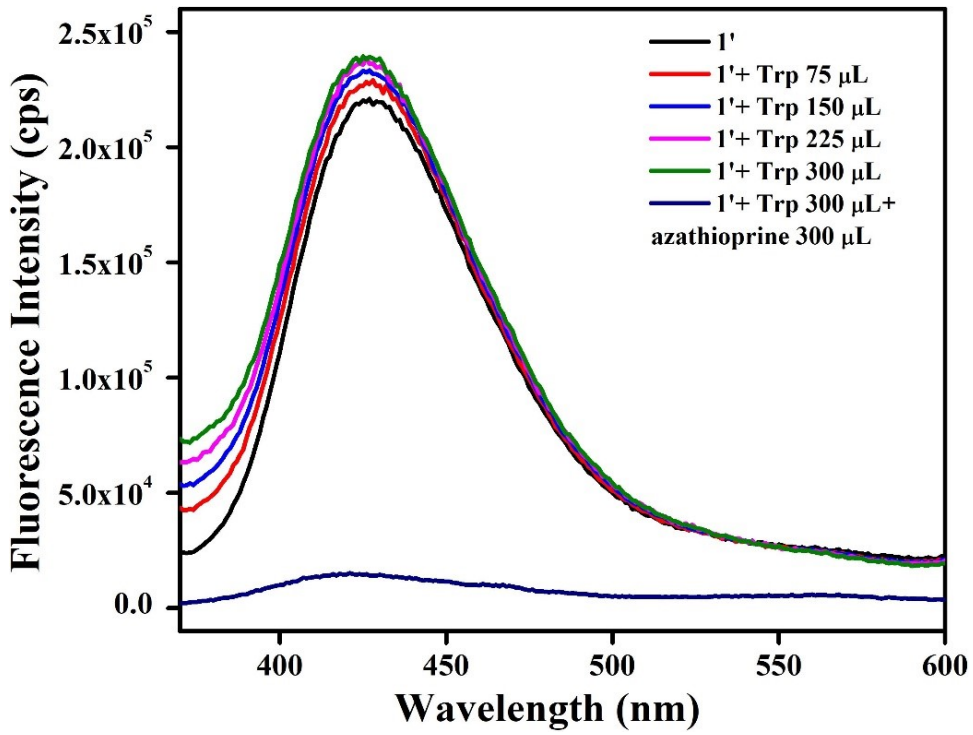

Figure S39. Fluorescence quenching intensity of the aqueous solution of **1′** after gradual addition of 300 µL of 5 mM aqueous tryptophan solution in presence of 300 µL of 5 mM solution of azathioprine.

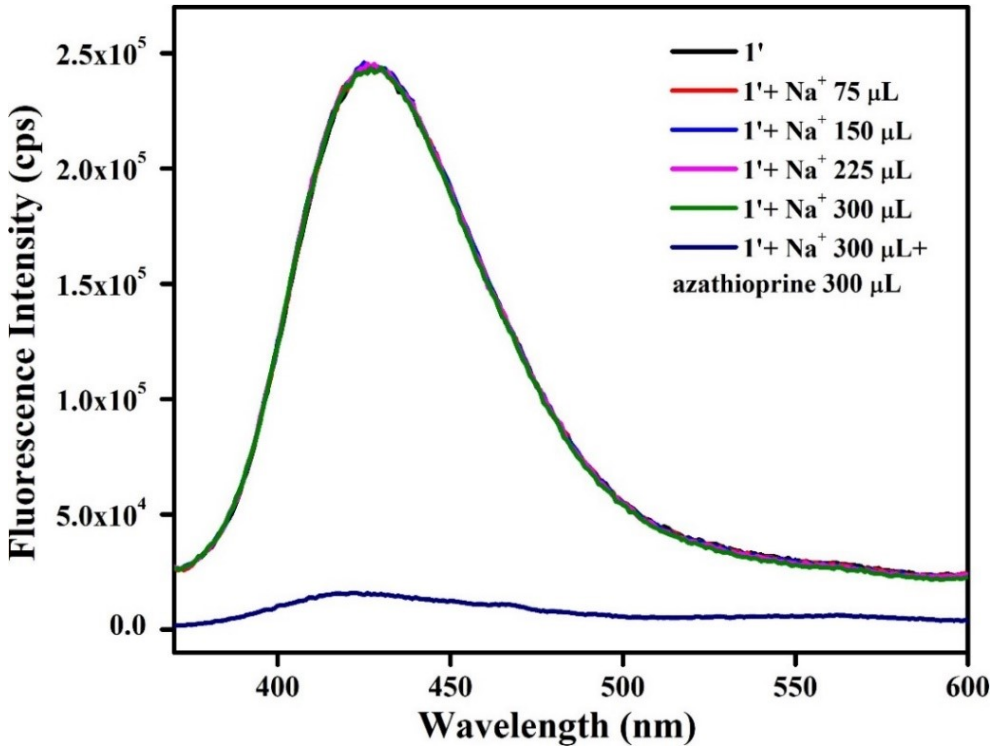

Figure S40. Fluorescence quenching intensity of the aqueous solution of **1′** after gradual addition of 300 µL of 5 mM aqueous Na^+ solution in the presence of 300 µL of 5 mM solution of azathioprine.

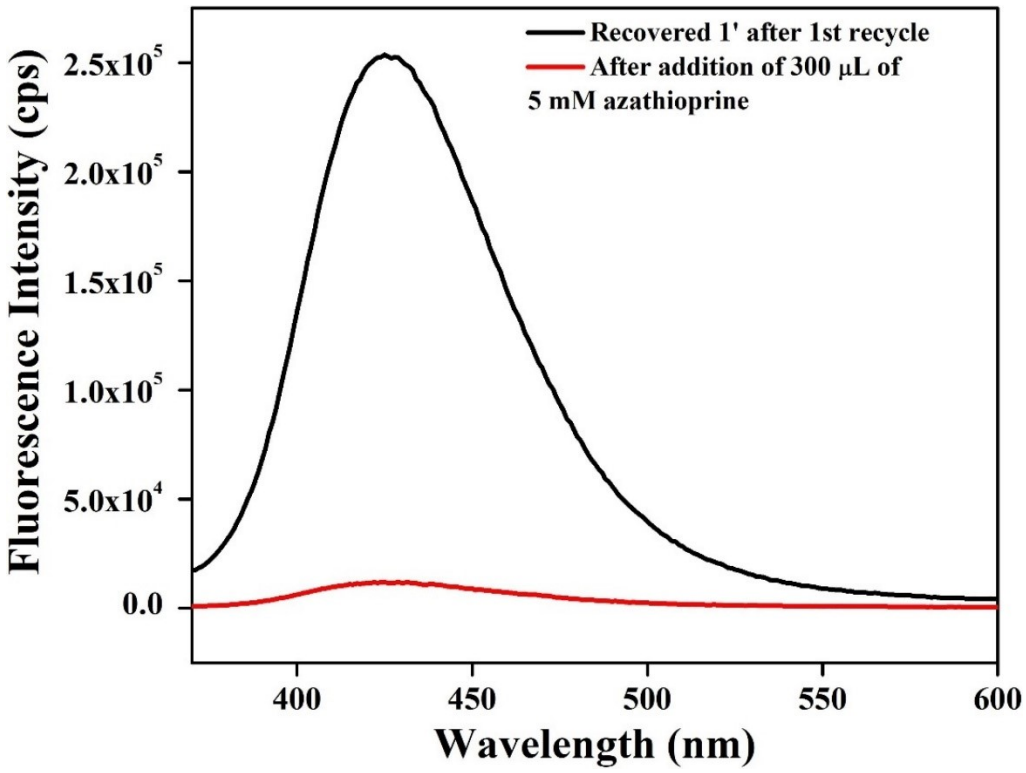

Figure S41. Photoluminescence spectrum for recyclability test of probe **1'** recovered from 1st cycle for the sensing of 5 mM azathioprine in aqueous medium.

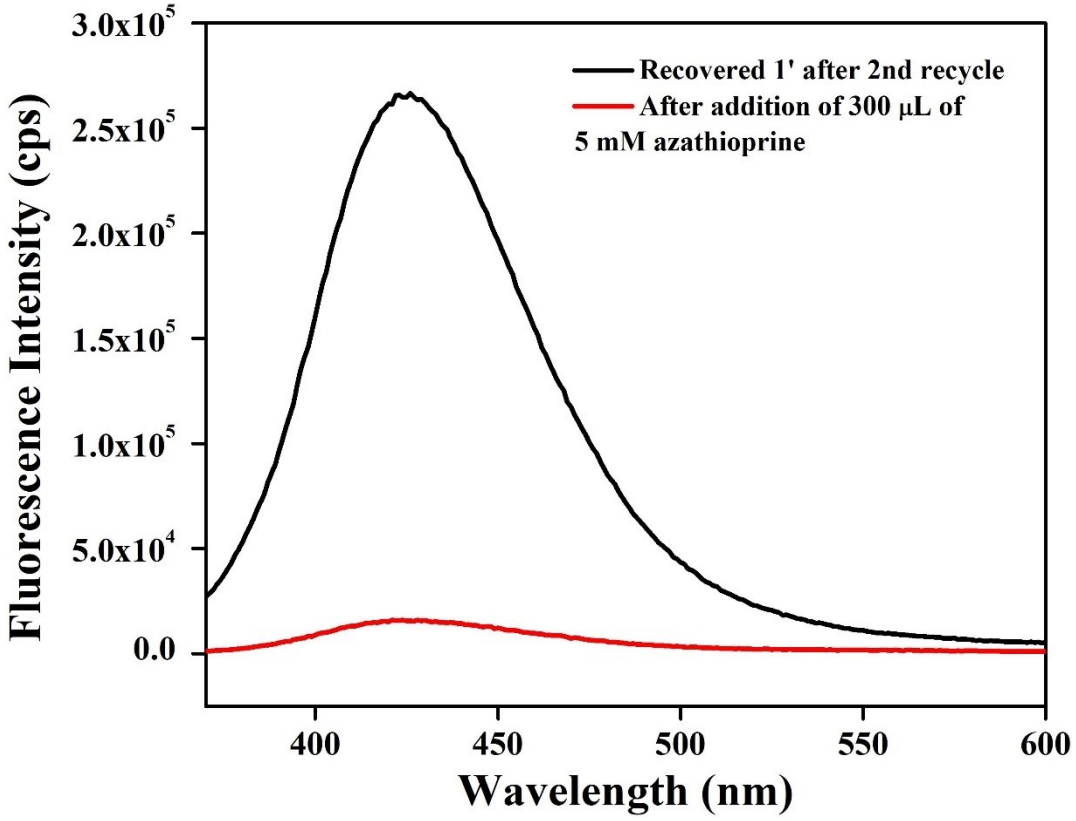

Figure S42. Photoluminescence spectrum for recyclability test of probe **1'** recovered from 2nd cycle for the sensing of 5 mM azathioprine in aqueous medium.

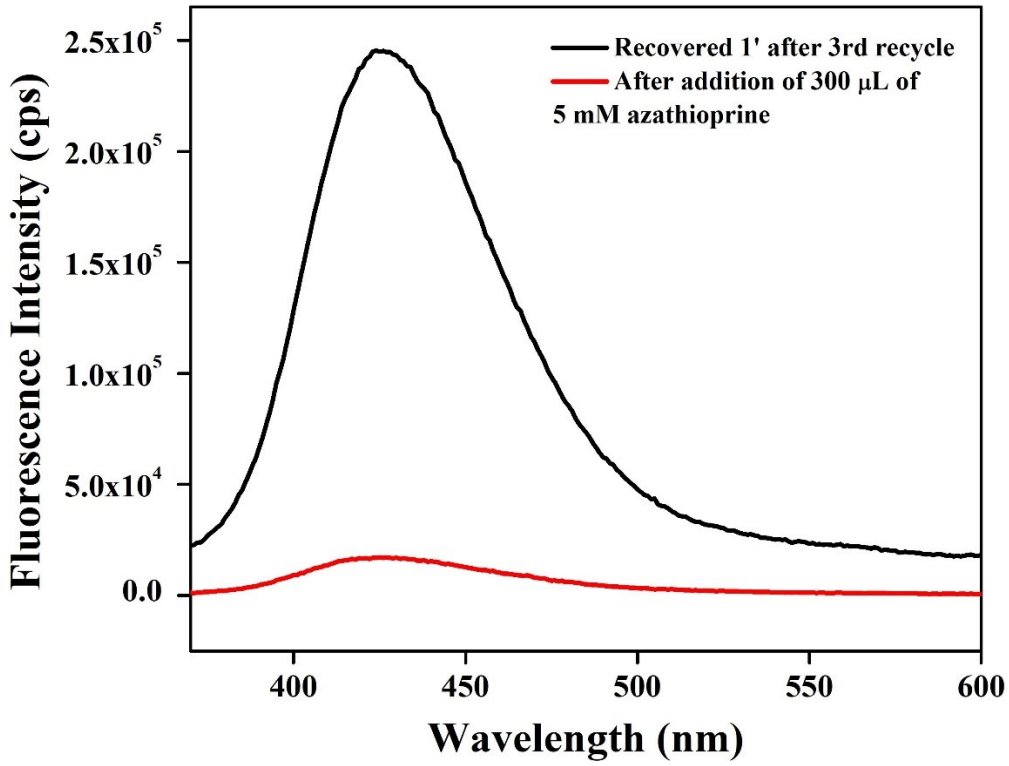

Figure S43. Photoluminescence spectrum for recyclability test of probe **1'** recovered from 3rd cycle for the sensing of 5 mM azathioprine in aqueous medium.

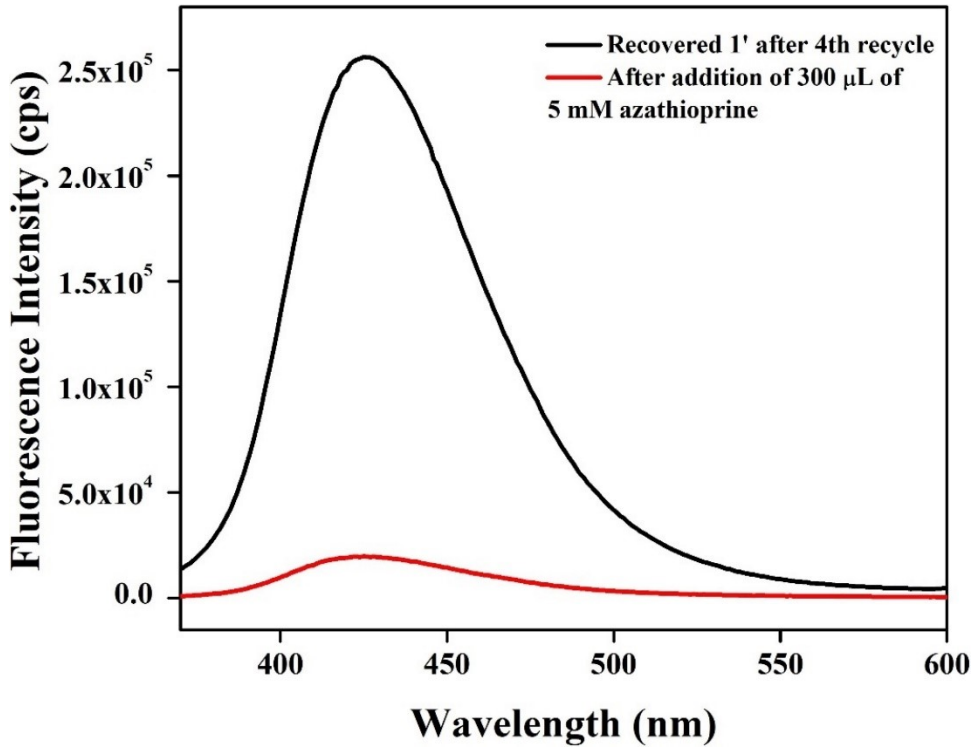

Figure S44. Photoluminescence spectrum for recyclability test of probe **1'** recovered from 4th cycle for the sensing of 5 mM azathioprine in aqueous medium.

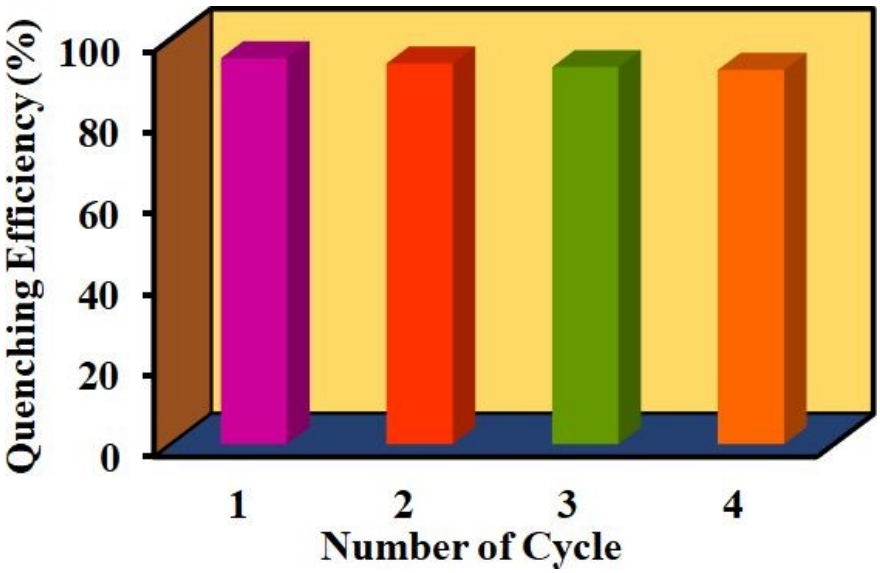

Figure S45. Recyclability test of probe **1'** for the sensing of 5 mM azathioprine in aqueous medium.

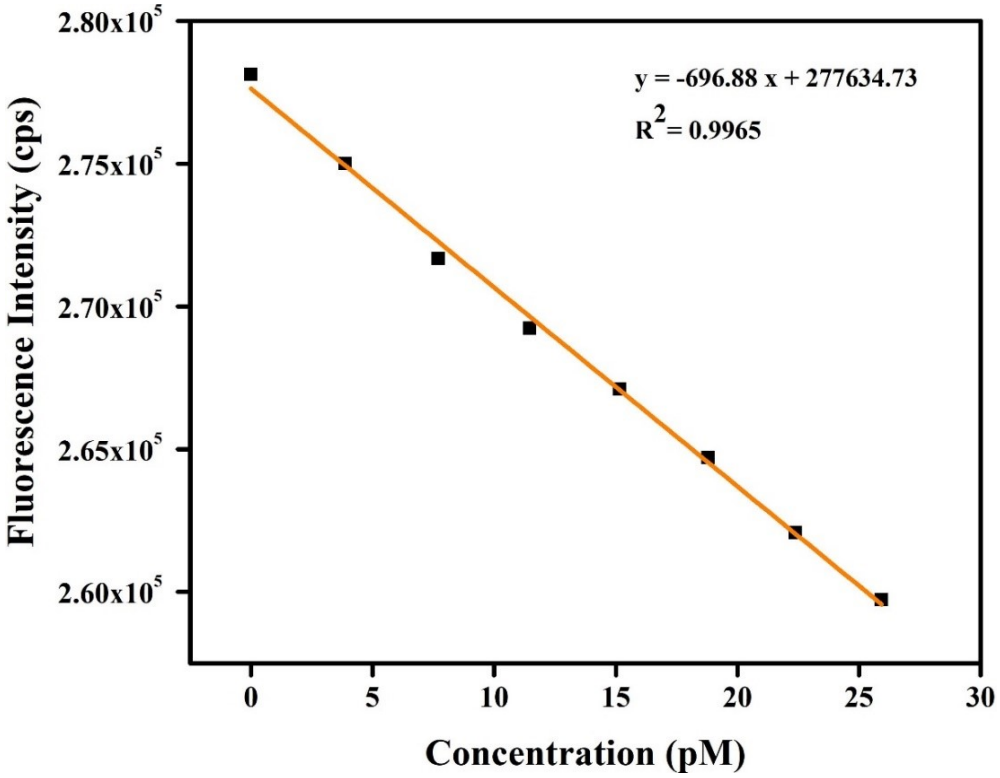

Figure S46. Change of fluorescence intensity of **1'** as a function of the concentration of azathioprine in water.

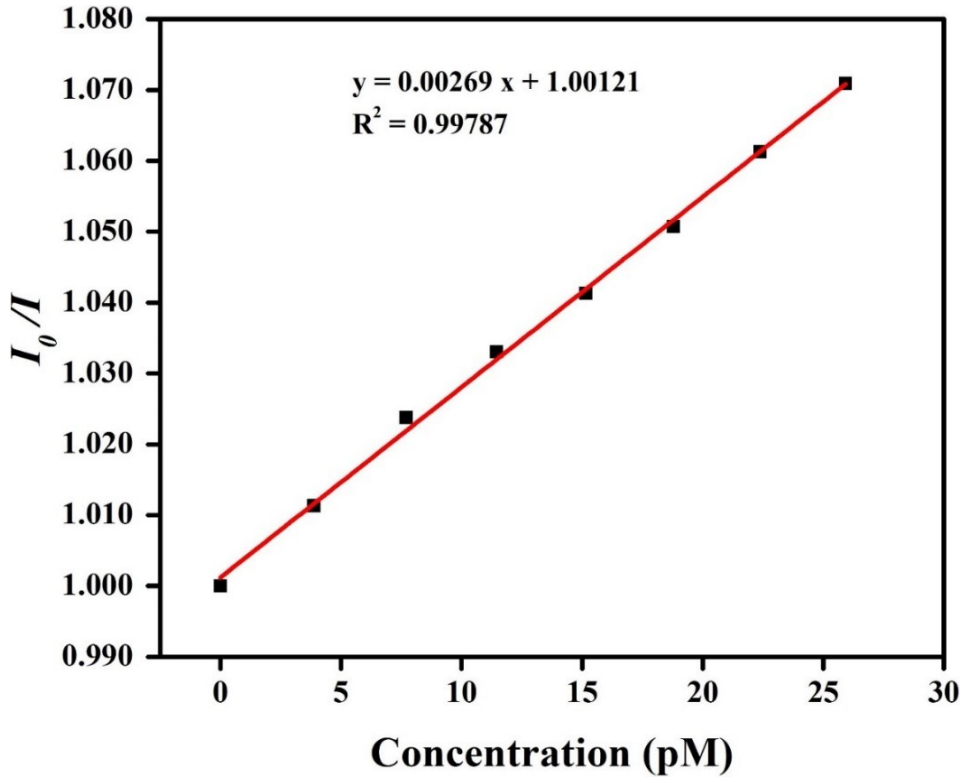

Figure S47. Stern-Volmer plot for the fluorescence quenching of **1'** in the presence of azathioprine in aqueous medium.

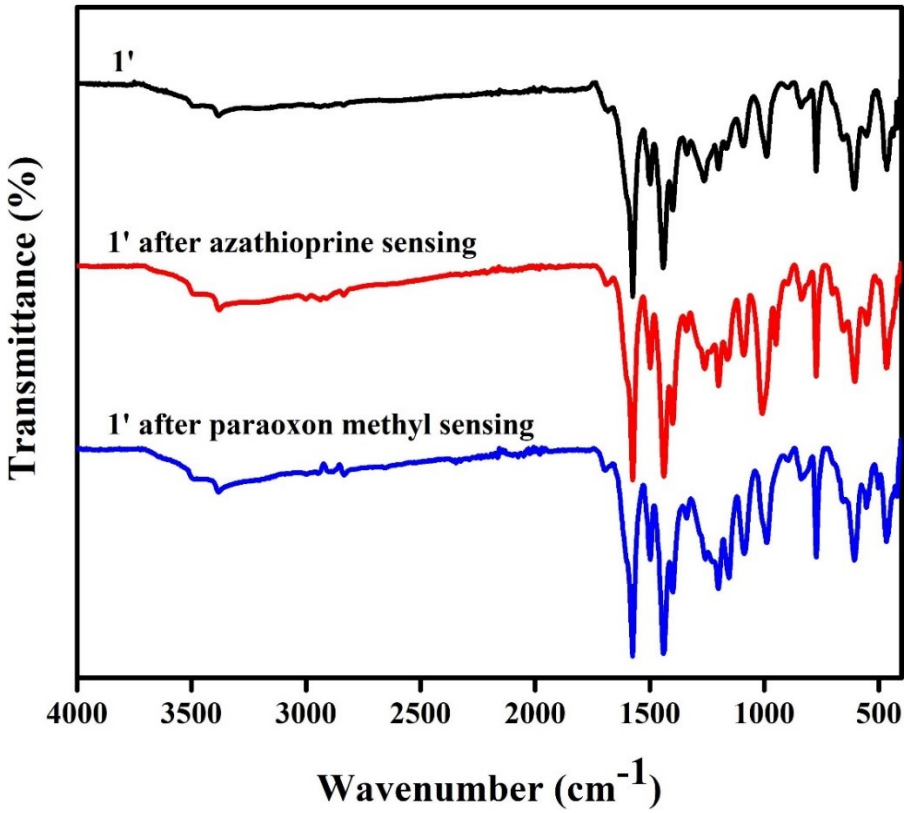

Figure S48. ATR-IR spectra of **1′** before sensing (black), after azathioprine sensing (red) and after paraoxon-methyl sensing (blue).

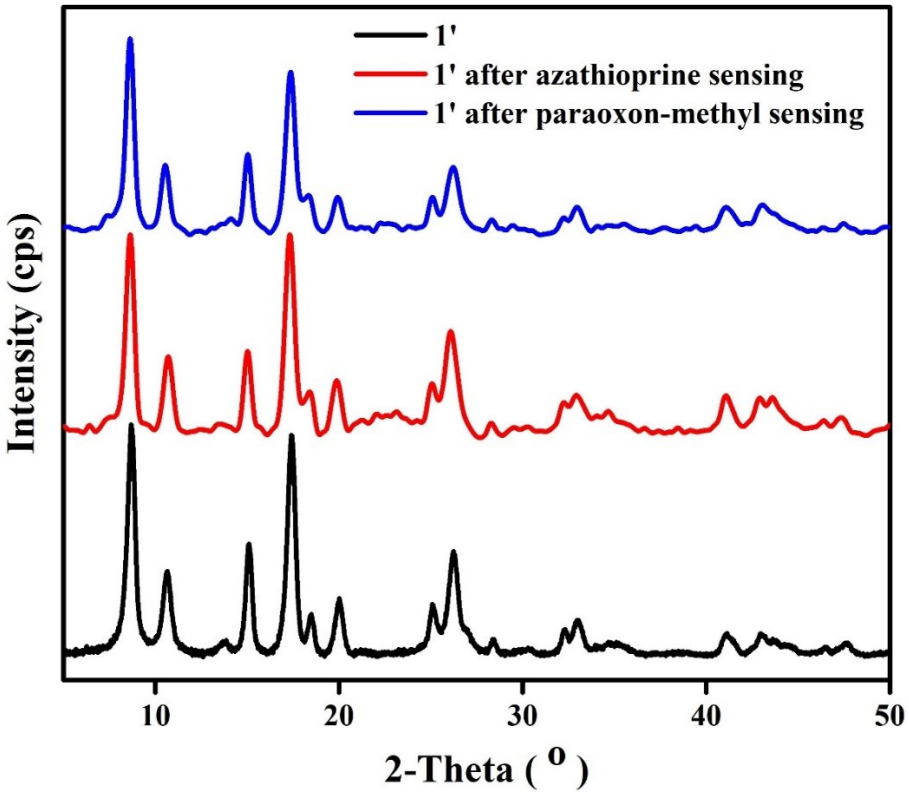

Figure S49. PXRD patterns of **1′** before sensing (black), after azathioprine sensing (red) and after paraoxon-methyl sensing (blue).

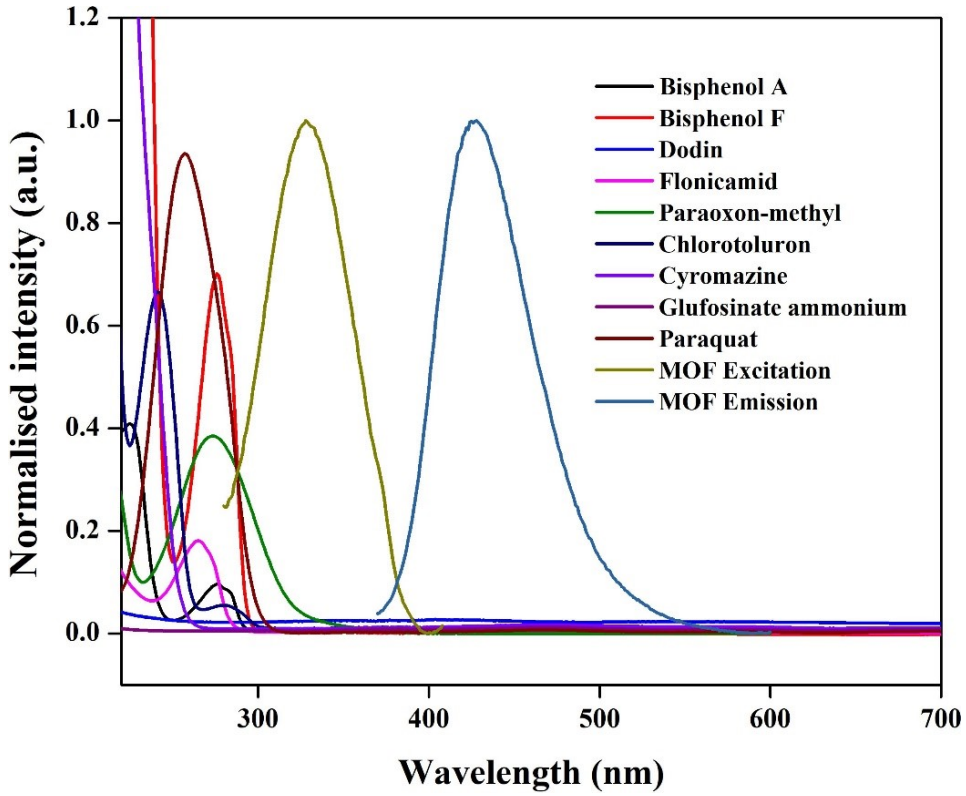

Figure S50. Overlap plot for UV-Vis spectra of all the analytes for paraoxon-methyl sensing with the fluorescence excitation and emission spectra of **1′**.

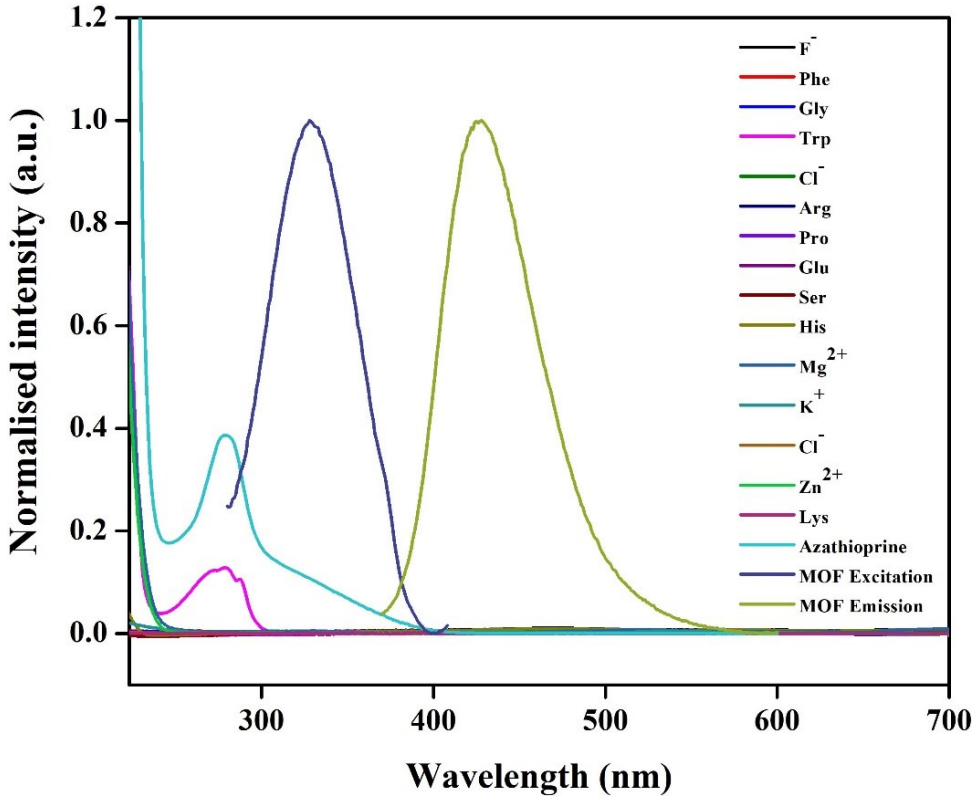

Figure S51. Overlap plot for UV-Vis spectra of all the analytes for azathioprine sensing with the fluorescence excitation and emission spectra of **1′**.

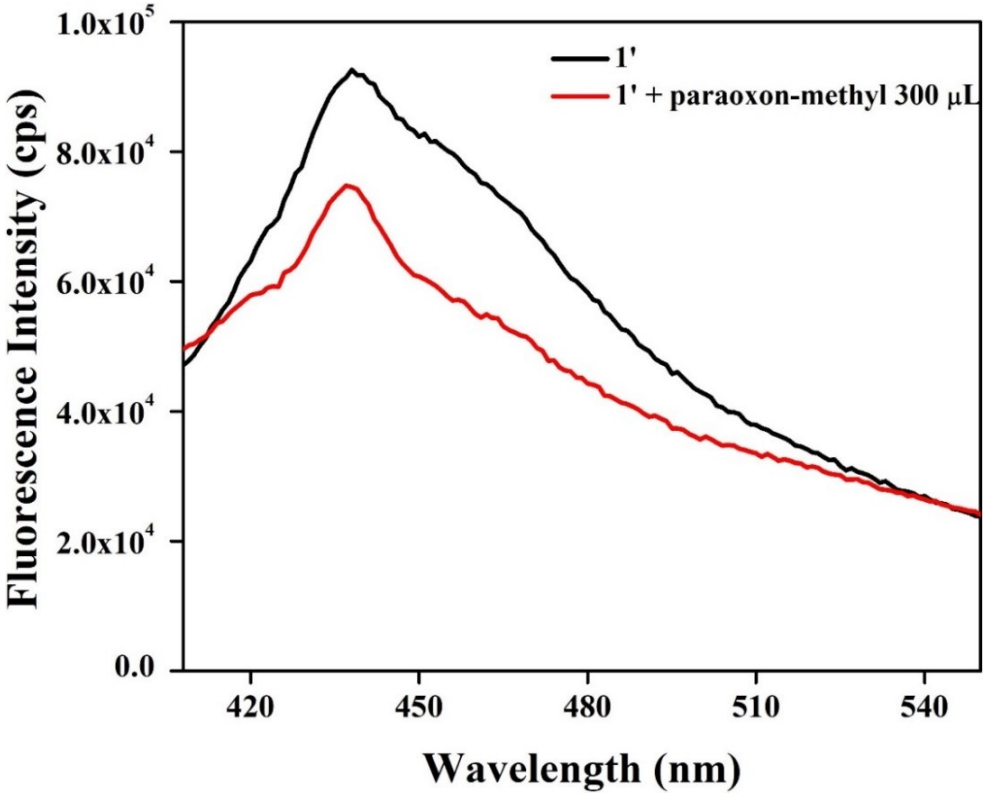

Figure S52. Photoluminescence spectrum of the aqueous solution of **1′** before and after addition of 300 µL of 5 mM paraoxon-methyl solution at 388 nm excitation.

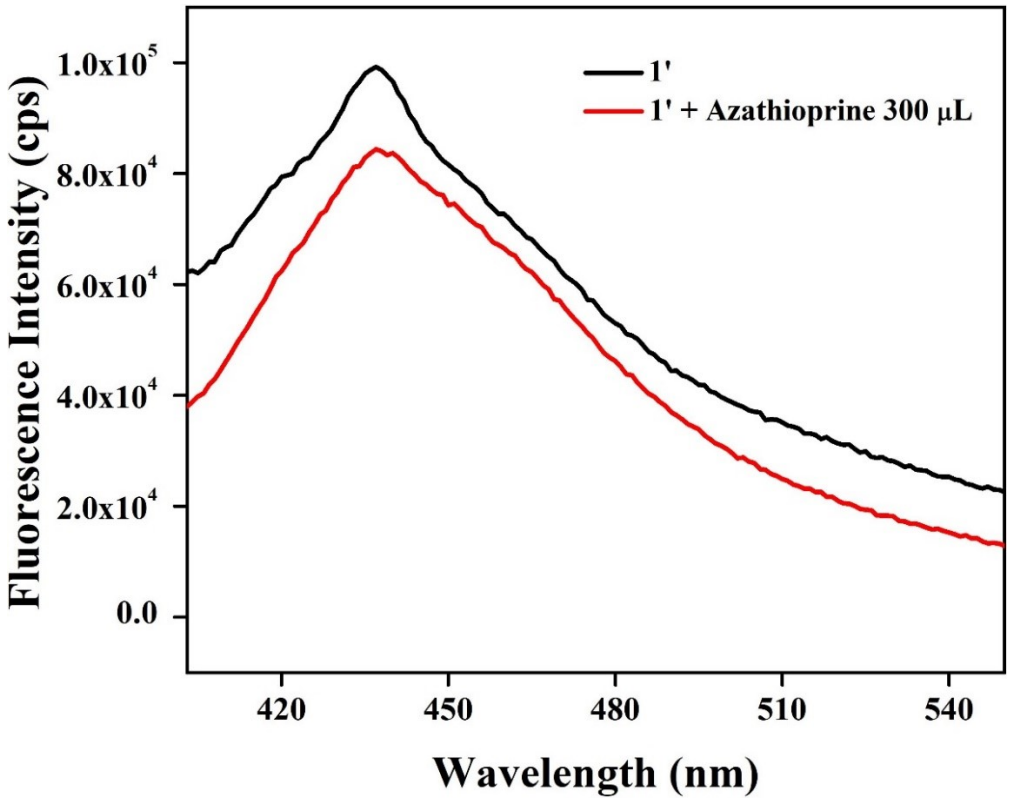

Figure S53. Photoluminescence spectra of the aqueous solution of **1′** before and after the addition of 300 µL of 5 mM azathioprine solution at 388 nm excitation.

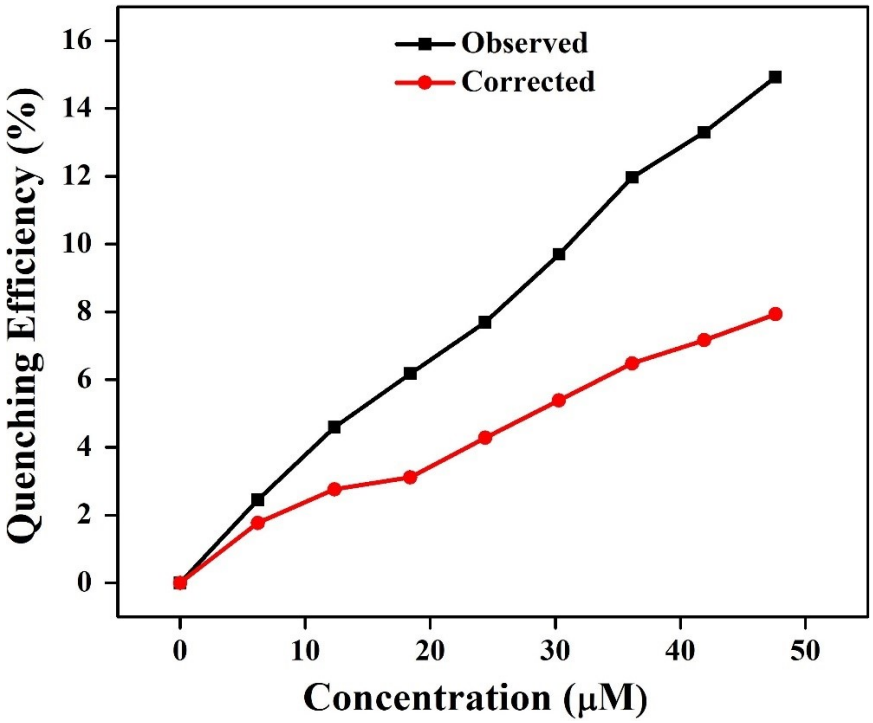

Figure S54. Quenching efficiency of observed (black curve) and corrected (red curve) measurements for **1′** after addition of paraoxon-methyl having different concentrations. Corrected quenching efficiency refers to the quenching efficiency when IFE contribution is not considered.

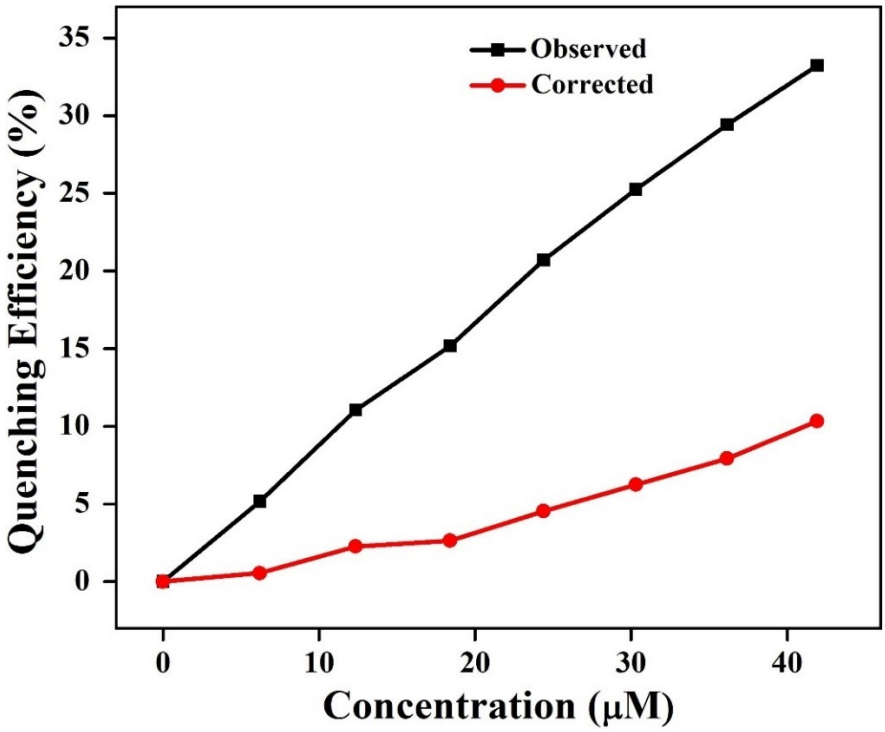

Figure S55. Quenching efficiency of observed (black curve) and corrected (red curve) measurements for **1′** after addition of azathioprine having different concentrations. Corrected quenching efficiency refers to the quenching efficiency when IFE contribution is not considered.

Table S3. Comparison of the response time, detection limit, K_{SV} and sensing media used for the reported sensors for azathioprine sensing.

Sl. No	Probe	Sensing Medium	K_{SV} (M^{-1})	LOD (pM)	Response Time (s)	Ref.
1	**$[Al(OH)(C_{16}H_{13}NO_6)]\cdot 0.5H_2O$**	**water**	**26.9×10^8**	**4.23**	**5**	**this work**
2	$AgBiS_2$/AGr composite by electrochemical methods	water	-	7×10^3	-	12
3	$Sm_2Sn_2O_7$ NPs by electrochemical methods	phosphate buffer	-	4×10^3	-	13
4	Spectrophotometry	water	-	-	-	14
5	Spectrophotometry	acetonitrile	-	2.15×10^6	-	15
6	AgNP	water	-	90×10^3	-	16
7	Spectrofluorometry	methanol	-	1.5×10^3	-	17

Table S4. IFE correction table for paraoxon-methyl sensing.

Paraoxon-methyl (μM)	**A_{ex}**	**A_{em}**	**Correction Factor (CF)**	**$F_{observed}$**	**$F_{corrected}$**	**$F_{corrected}(0)/F_{corrected}$**
0	0.1530	0.1209	1.3268	272814.2249	361962.9047	1
6.21	0.1581	0.1225	1.3359	266145.6044	355563.3512	1.0179
12.35	0.1692	0.1226	1.3523	260280.3628	351968.7863	1.0284
18.40	0.1789	0.1255	1.3701	255959.5438	350687.7385	1.0322
24.39	0.1818	0.1265	1.3757	251845.1419	346470.7553	1.0447
30.30	0.1890	0.1293	1.3901	246349.7739	342465.5594	1.0569
36.14	0.2018	0.1295	1.4095	240163.4810	338506.0283	1.0693
41.92	0.2080	0.1308	1.4206	236546.9155	336033.1385	1.0772
47.62	0.2150	0.1343	1.4359	232099.0396	333270.5729	1.0861

Table S5. IFE correction table for paraoxon-azathioprine sensing.

Azathioprine (μM)	**A_{ex}**	**A_{em}**	**Correction Factor (CF)**	**$F_{observed}$**	**$F_{corrected}$**	**$F_{corrected}(0)/F_{corrected}$**
0	0.0533	0.0469	1.1086	258924.1456	287033.5867	1
6.21	0.0955	0.0472	1.1625	245563.7790	285462.6246	1.0055
12.35	0.1379	0.0473	1.2181	230314.1176	280536.1321	1.0232
18.40	0.1766	0.0493	1.2724	219620.3617	279452.9985	1.0271
24.39	0.2209	0.0499	1.3346	205301.5780	273994.1493	1.0476
30.30	0.2601	0.0499	1.3904	193555.3321	269118.2866	1.0666
36.14	0.2976	0.0507	1.4463	182726.5099	264269.5498	1.0861
41.92	0.3261	0.0509	1.4889	172872.9461	257388.9597	1.1152

References:

1. Das, A.; Das, A. K., A functionalized Hf (iv)–organic framework introducing an efficient, recyclable, and size-selective heterogeneous catalyst for MPV reduction. *New J. Chem.* **2023,** *47* (11), 5347-5355.
2. *Materials Studio Version 5.0.* , Accelrys Inc.: San Diego, 2009.
3. M. J. Frisch, G. W. T., H. B. Schlegel, G. E. Scuseria, M. A. Robb, J. R. Cheeseman, G. Scalmani, V. Barone, G. A. Petersson, H. Nakatsuji, X. Li, M. Caricato, A. Marenich, J. Bloino, B. G. Janesko, R. Gomperts, B. Mennucci, H. P. Hratchian, J. V. Ortiz, A. F. Izmaylov, J. L. Sonnenberg, D. Williams-Young, F. Ding, F. Lipparini, F. Egidi, J. Goings, B. Peng, A. Petrone, T. Henderson, D. Ranasinghe, V. G. Zakrzewski, J. Gao, N. Rega, G. Zheng, W. Liang, M. Hada, M. Ehara, K. Toyota, R. Fukuda, J. Hasegawa, M. Ishida, T. Nakajima, Y. Honda, O. Kitao, H. Nakai, T. Vreven, K. Throssell, J. A. Montgomery, Jr., J. E. Peralta, F. Ogliaro, M. Bearpark, J. J. Heyd, E. Brothers, K. N. Kudin, V. N. Staroverov, T. Keith, R. Kobayashi, J. Normand, K. Raghavachari, A. Rendell, J. C. Burant, S. S. Iyengar, J. Tomasi, M. Cossi, J. M. Millam, M. Klene, C. Adamo, R. Cammi, J. W. Ochterski, R. L. Martin, K. Morokuma, O. Farkas, J. B. Foresman, and D. J. Fox, Gaussian 09, Revision A.02. *Gaussian, Inc., Wallingford CT* **2016.**
4. Boultif, A.; Louer, D., Indexing of powder diffreaction patterns for low-symmetry lattices by the successive dichotomy method. *J. Appl. Crystallogr.* **1991,** *24*, 987-993.
5. Meilikhov, M.; Yusenko, K.; Fischer, R. A., The adsorbate structure of ferrocene inside [Al (OH)(bdc)] x (MIL-53): a powder X-ray diffraction study. *Dalton Trans.* **2009,** (4), 600-602.
6. Luo, M.; Wei, J.; Zhao, Y.; Sun, Y.; Liang, H.; Wang, S.; Li, P., Fluorescent and visual detection of methyl-paraoxon by using boron-and nitrogen-doped carbon dots. *Microchemical journal* **2020,** *154*, 104547.
7. Luo, M.; Chen, L.; Wei, J.; Cui, X.; Cheng, Z.; Wang, T.; Chao, I.; Zhao, Y.; Gao, H.; Li, P., A two-step strategy for simultaneous dual-mode detection of methyl-paraoxon and Ni (II). *Ecotoxicol. Environ. Saf.* **2022,** *239*, 113668.
8. Dewangan, L.; Korram, J.; Karbhal, I.; Nagwanshi, R.; Ghosh, K. K.; Pervez, S.; Satnami, M. L., Alkaline phosphatase immobilized CdTe/ZnS quantum dots for dual-purpose fluorescent and electrochemical detection of methyl paraoxon. *Ind. Eng. Chem. Res.* **2022,** *61* (10), 3636-3646.
9. Li, N.; Yu, Y.; Zhou, Y.; Xu, K.; Zhou, Y.; Zhang, L.; Zhong, Y., Construction of a logic gate computation and visual test paper for methyl paraoxon assay based on a fluorescent europium–organic framework. *J. Mater. Chem. C* **2024,** *12* (7), 2493-2504.
10. Li, Y.; Huang, Z.; Liu, B.; Huang, Z.-Z.; Yang, H.; Tan, H., Portable hydrogel test kit integrated dual-emission coordination polymer nanocomposite for on-site detection of organophosphate pesticides. *Biosens. Bioelectron.* **2023,** *220*, 114890.
11. Wang, J.; Zhang, J.; Wang, J.; Fang, G.; Liu, J.; Wang, S., Fluorescent peptide probes for organophosphorus pesticides detection. *J. Hazard. Mater.* **2020,** *389*, 122074.
12. Alagumalai, K.; Sivakumar, M.; Kim, S.-C.; Babulal, S. M.; Ouladsmane, M., AgBiS2 embedded activated graphene nanolayer for sensing azathioprine in biospecimens. *Colloids Surf. A Physicochem. Eng. Asp.* **2024,** *685*, 133243.

13. Rajakumaran, R.; Balamurugan, K.; Chen, S.-M.; Sukanya, R.; Breslin, C. B., Electrocatalytic studies of coral-shaped samarium stannate nanoparticles for selective detection of azathioprine in biological samples. *ACS Appl. Nano Mater.* **2021,** *4* (12), 13048-13059.
14. Bhaskar, M.; Manohara, Y.; Gayasuddin, M.; Balaraju, M.; Kumar, T. B., Spectrophotometric determination of azathioprine in bulk and pharmaceutical dosage forms. *Int. J. Chemtech Res.* **2010,** *2* (1), 376-378.
15. Ramachandra, B.; Naidu, N. V., UV-Visible Spectrophotometric method for the determination of azathioprine. *J. pharm. biol. sci.* **2016,** *4* (6), 179.
16. Rezaei, Z. B.; Rastegarzadeh, S.; Kiasat, A., In-situ decorated silver nanoparticles on electrospun poly (vinyl alcohol)/chitosan nanofibers as a plasmonic sensor for azathioprine determination. *Colloids Surf. A Physicochem. Eng. Asp.* **2018,** *559*, 266-274.
17. Almahri, A. M.; Jabli, M., Successful spectrofluorometric and chemiluminescence methods for the estimation of azathioprine as an immunosuppressive drug in pharmaceutical preparation. *Arab. J. Chem.* **2020,** *13* (12), 8708-8716.